ANALYTICAL TOOLS FOR RESILIENCE OF LIFELINE HIGHWAY BRIDGES TO TSUNAMI EVENTS

FINAL PROJECT REPORT

by

Michael H. Scott
Oregon State University

Sponsorship
PacTrans and Oregon DOT

for

Pacific Northwest Transportation Consortium (PacTrans)
USDOT University Transportation Center for Federal Region 10
University of Washington
More Hall 112, Box 352700
Seattle, WA 98195-2700

In cooperation with US Department of Transportation-Research and Innovative Technology Administration (RITA)

Disclaimer

The contents of this report reflect the views of the authors, who are responsible for the facts and the accuracy of the information presented herein. This document is disseminated under the sponsorship of the U.S. Department of Transportation's University Transportation Centers Program, in the interest of information exchange. The Pacific Northwest Transportation Consortium, the U.S. Government and matching sponsor assume no liability for the contents or use thereof.

Technical Report Documentation Page

1. Report No.	2. Government Accession No.	3. Recipient's Catalog No.

4. Title and Subtitle	5. Report Date
ANALYTICAL TOOLS FOR RESILIENCE OF LIFELINE HIGHWAY BRIDGES TO TSUNAMI EVENTS	August 30, 2018
	6. Performing Organization Code
7. Author(s) Michael H. Scott, Oregon State University	**8. Performing Organization Report No.**
9. Performing Organization Name and Address PacTrans Pacific Northwest Transportation Consortium University Transportation Center for Federal Region 10 University of Washington More Hall 112 Seattle, WA 98195-2700	**10. Work Unit No. (TRAIS)** **11. Contract or Grant No.** DTRT13-G-UTC40
12. Sponsoring Organization Name and Address United States of America DEPARTMENT OF TRANSPORTATION Office of the Assistant Secretary for Research and Technology	**13. Type of Report and Period Covered** **14. Sponsoring Agency Code**

15. Supplementary Notes
Report uploaded at www.pacTrans.org

16. Abstract
Extreme tsunami events in the 21st century, particularly the 2004 Indian Ocean and 2011 Great East Japan events, have put the vulnerability of coastal transportation infrastructure to tsunamis at the front of bridge engineering design and assessment. The 2011 Japan event was particularly eye-opening because its infrastructure was designed to resist very high seismic risk; however, many bridges were washed away or rendered unserviceable due to wave loading. In response to these events, several experimental and analytical research projects have been undertaken to improve the resilience of transportation infrastructure to tsunami attack. Detailed, time consuming analyses are required to capture fluid-structure interaction during tsunami runup and inundation and the results are highly variable due to uncertain boundary conditions and uncertain wave loading scenarios. The intended result of these experiments and analyses is, among other things, to develop loading equations for engineers to quickly assess the impact of tsunami loading on bridges. In this project, simplified analytical models and loading conditions are developed in order to estimate horizontal tsunami loads on bridge superstructures. Comparisons are made with wave flume experiments made available by the Public Works Research Institute (PWRI) in Japan. In addition, the role of connections and/or substructure flexibility is explored and response spectra are developed. The results indicate the simplified approach reasonably predicts peak horizontal forces, but without any clear trends. As expected, the simplified analyses are not able to capture high intensity impact forces owing to pressure shocks. In addition, as the natural period of the bridge system increases, e.g., due to added flexibility, the forces in the connections and/or substructure tend to increase. Again, the simplified analysis ignores the interaction of structure and fluid as flexibility is added to the system. The simple analytical approach offers a framework for developing and refining tsunami loading equations and it can also be applied to equations for uplift and downward force.

17. Key Words	18. Distribution Statement
Bridges, Tsunamis, Fluid-Structure Interaction, Analysis, Loads	No restrictions.

19. Security Classification (of this report)	20. Security Classification (of this page)	21. No. of Pages	22. Price
Unclassified.	Unclassified.	56	NA

Contents

List of Figures

Acknowledgments

This project was an outcropping of a transportation pooled fund study, TPF-5(307), on the development of bridge design guidelines for tsunami loading. The TPF study was sponsored by the Pacific states of Oregon, California, Washington, Alaska, and Hawaii. The state support and the technical expertise of bridge engineers from each state is gratefully acknowledged along with the project management efforts of Jon Lazarus from Oregon DOT and technical and administrative support of Steve Mahin and Yousef Bozorgnia from the Pacific Earthquake Engineering Research (PEER) center. The expertise offered by Patrick Lynett from the University of Southern California, the PI of the TPF study, and the contributions of other researchers, who lent their insights on a volunteer basis, were of tremendous benefit to both the TPF study and this project. The experimental data shared by Jun-ichi Hoshikuma from the Public Works Research Institute (PWRI) was instrumental in this project and the TPF study. Finally, this project would not have been possible without support from PacTrans and the coordination efforts of David Hurwitz from Oregon State University and Christina Yarbrough from the University of Washington.

Executive Summary

Extreme tsunami events in the 21st century, particularly the 2004 Indian Ocean and 2011 Great East Japan events, have put the vulnerability of coastal transportation infrastructure to tsunamis at the front of bridge engineering design and assessment. The 2011 Japan event was particularly eye-opening because its infrastructure was designed to resist very high seismic risk; however, many bridges were washed away or rendered unserviceable due to wave loading. In response to these events, several experimental and analytical research projects have been undertaken to improve the resilience of transportation infrastructure to tsunami attack. Detailed, time consuming analyses are required to capture fluid-structure interaction during tsunami runup and inundation and the results are highly variable due to uncertain boundary conditions and uncertain wave loading scenarios. The intended result of these experiments and analyses is, among other things, to develop loading equations for engineers to quickly assess the impact of tsunami loading on bridges. In this project, simplified analytical models and loading conditions are developed in order to estimate horizontal tsunami loads on bridge superstructures. Comparisons are made with wave flume experiments made avaialble by the Public Works Research Institute (PWRI) in Japan. In addition, the role of connections and/or substructure flexibility is explored and response spectra are developed. The results indicate the simplified approach reasonably predicts peak horizontal forces, but without any clear trends. As expected, the simplified analyses are not able to capture high intensity impact forces owing to pressure shocks. In addition, as the natural period of the bridge system increases, e.g., due to added flexibility, the forces in the connections and/or substructure tend to increase. Again, the simplified analysis ignores the interaction of structure and fluid as flexibility is added to the system. The simple analytical approach offers a framework for developing and refining tsunami loading equations and it can also be applied to equations for uplift and downward force.

1 Introduction

Highway bridges serve as critical lifelines after natural disasters such as earthquakes and tsunamis. While earthquakes over the last quarter century, e.g., Loma Prieta and Northridge, have led to rapid evolution of design codes for buildings and bridges, the less frequent but potentially more catastrophic threat of a tsunami has come to the forefront of resilience-based design for coastal infrastructure. The 2004 Indian Ocean tsunami exposed the vulnerability of coastal infrastructure and lifelines in many southeast Asian countries while the 2011 tsunami that struck the east coast of Japan reinforced the fact that countries with modern design standards, based primarily on seismic hazards that exceed those in the United States, are at significant risk for damage and total loss from tsunami inundation.

Geologic conditions similar to those found off the east coast of Japan are also present off the west coast of the United States. The Cascadia subduction zone (CSZ) poses a direct threat for a major tsunami that could impact the coastlines of Oregon, Washington, and northern California. The CSZ last triggered an earthquake and subsequent tsunami about 400 years ago and has a high probability of unleashing a similar event in the next 100 years. The ability of bridges along the Oregon and Washington coasts to resist the demands posed by forecast tsunami events is in doubt and research is underway to address this issue.

To assess and design bridges to resist tsunami attack, engineers require simplified approaches for estimating the loads. Tsunami loading owing to seawater alone consists of hydrostatic and hydrodynamic components. Debris-laden seawater, the impact of waterborne debris, and debris damming effects can lead to significant increases in tsunami loads; however, they will not be addressed herein. Detailed numerical simulations and comparisons with experimental data shed light on the development of loading equations.

2 Literature Review

Several experimental programs for tsunami loading on bridges have been completed in the last decade. Hayatdavoodi et al [1] performed 1:35 scale experiments for a wide range of water depths, wave amplitudes, submergence depths, and elevations for solitary wave loads on deck-girder bridges. Wave flume experiments were conducted by Hoshikuma et al [2] at PWRI in Japan on 1:20 scale deck-girder bridge models that varied in deck overhang, number of girders, and girder spacing. Additional PWRI experiments examined protective strategies (fairings and pedestrian bridges) for the mitigation of tsunami-induced forces [3]. The effects of deck skew, deck venting to release trapped air, and connection flexibility were investigated in experiments by Istrati et al [4, 5] on 1:5 scale bridge models for both broken and unbroken waves on I-girder bridges with cross frames, solid diaphragms, and soffit slab. Experiments to determine bridge response to non-tsunami wave loading, e.g., from wind storms, have also been conducted [6, 7].

The aforementioned researchers developed computational models that matched their experimental results reasonably well. Due to the cost of experiments, researchers have also used completely simulation-based approaches to determine the effects of tsunami wave loading on bridges. Bricker et al [8] used the OpenFOAM CFD program to examine the effects of lift, drag, and moment forces on a typical bridge deck caused by tsunami bores and smoothly rising flows. Azadbakht and Yim [9] used LS-DYNA to compute horizontal and vertical loads and overturning moments on bridges for a hypothetical CSZ event. The effects of bridge deck skew and superelevation were examined by detailed three-dimensional analysis in OpenFOAM by Motley et al [10]. Such simulations are essential for designing new experiments and for preliminary examination of protective strategies to mitigate bridge damage from tsunami loading. While these published simulation results were correlated with previous experimental data, large variances were observed in blind prediction of the PWRI experimental results by multiple researchers at a 2014 workshop

on tsunami load simulation [11]. Workshop participants employed a wide range of sophisticated FSI simulation strategies; however, there was consensus on the need for simplified modeling approaches.

Azadbakht and Yim [12] developed loading equations based on a series of simulations for hypothetical CSZ events on Oregon bridges. The equations consisted of hydrostatic and hydrodynamic components and were based on scenarios of tsunami runup and full inundation. Additional research is underway to determine refinements to these loading equations for the development of bridge design guidelines for tsunami loading [13].

3 Simplified Analytical Model

With numerous previous efforts at detailed CFD simulations of bridge response to tsunami loading, the approach taken herein is based on a simplified representation of a bridge superstructure as a single degree-of-freedom (SDF) mass-spring-damper system. While bridge superstructures typically act as rigid objects connected to the substructure, the SDF mass-spring-damper system enables the assessment of design and mitigation strategies, namely the addition of flexible connections to the substructure.

Single degree-of-freedom (SDF) models similar to the one described in this chapter are frequently used in the design and assessment of structures to resist seismic loading. Response spectra are generated from SDF models in order to inform engineers of the changes in structural response to an earthquake ground motion expected from a change in mass or stiffness of the structure. Herein, instead of an earthquake ground motion, the input forcing function applied to the SDF system is based on time histories of wave height and speed. However, unlike earthquake loading where the external forcing function is proportional to structural mass and the equation of motion can be normalized, knowledge of the bridge dimensions and mass must be taken in to account when generating hydrodynamic loads on the SDF system. As a result, the actual bridge mass and depth will be used throughout the analyses herein.

The connection between a bridge superstructure and its substructure is typically very stiff, making the natural period of the systems explored herein very short. This results in what is essentially a rigid object; however, the framework of a mass-spring-damper system permits the exploration of mitigation strategies for reducing the effects of horizontal forces on bridge superstructures, e.g., through flexible bearings. The analyses also show the effect of stiffness on the forces developed in the substructure.

3.1 Model Description

The simplified analytical model of a mass-spring-damper system is shown in figure 3.1 where m is the system mass, k is the spring stiffness, and c is the dashpot damping coefficient.

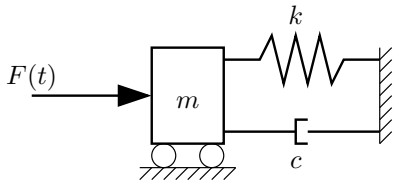

Figure 3.1: Single degree-of-freedom analytical model of mass-spring-damper system.

The undamped natural period of vibration for this analytical model is

$$T_n = 2\pi\sqrt{\frac{m}{k}} \tag{3.1}$$

while for damped vibration, the natural period is

$$T_D = \frac{T_n}{\sqrt{1-\xi^2}} \tag{3.2}$$

where $\xi = c/(2m\omega_n)$ is the damping ratio with respect to critical damping, i.e., damping that is sufficient to prevent oscillation. For lightly damped systems ($\xi < 0.2$), the damped natural period is approximately equal to the undamped natural period.

The forcing function, $F(t)$ shown in figure 3.1, is postulated as the sum of hydrodynamic and hydrostatic components

$$F(t) = F_d(t) + F_s(t) \tag{3.3}$$

The time history of hydrodynamic force, $F_d(t)$, is computed as

$$F_d(t) = \frac{1}{2}C_d\rho Bh(t)u(t)^2 \tag{3.4}$$

where C_d is the drag coefficient, ρ is the fluid density, and B is the out-of-plane width of the object. The time series of flow speed, $u(t)$, is assumed to be uniform across the height of the object. The time series of flow height across the object, $h(t)$, depends on the wave height, $H(t)$, relative to the vertical position of the object, as shown in figure 3.2.

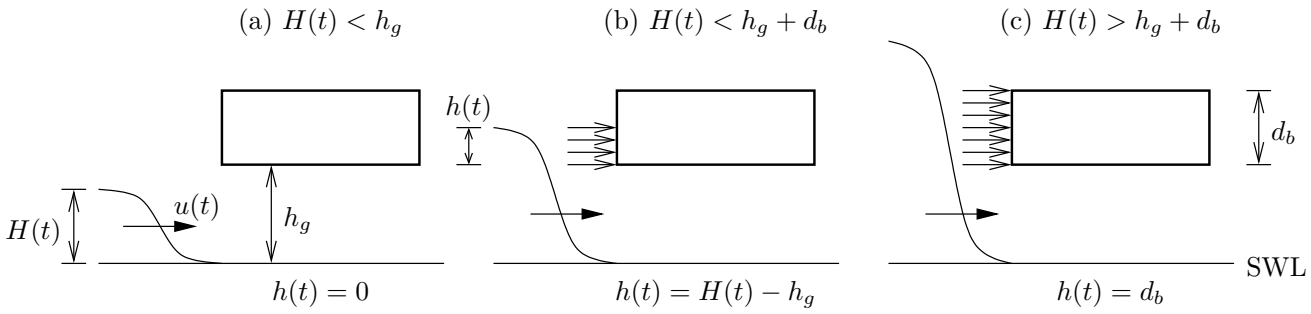

Figure 3.2: Flow height across object for hydrodynamic force calculation: (a) flow below object; (b) flow on object; and (c) flow above object.

The time history of hydrostatic force, $F_s(t)$, is based on the average hydrostatic pressure applied to the face of the object.

$$F_s(t) = \frac{1}{2}(p_1(t) + p_2(t))(Bh(t)) \tag{3.5}$$

where $p_1(t)$ and $p_2(t)$ are the pressures on the object face (figure 3.3), B is the out-of-plane length of the object, and $h(t)$ is the flow height across the object. The hydrostatic pressures are based on the flow conditions

$$p(t) = \rho g d(t) \tag{3.6}$$

where $d(t)$ is the fluid depth to the point where the pressure is computed, as shown in figure 3.3 for three cases of fluid flow. It is noted that hydrostatic loading is only applied to the front face of the bridge. After inundation, fluid will envelop the bridge and produce opposing hydrostatic forces on the back of the bridge; however, this effect is beyond the

scope of the simplified approach presented herein.

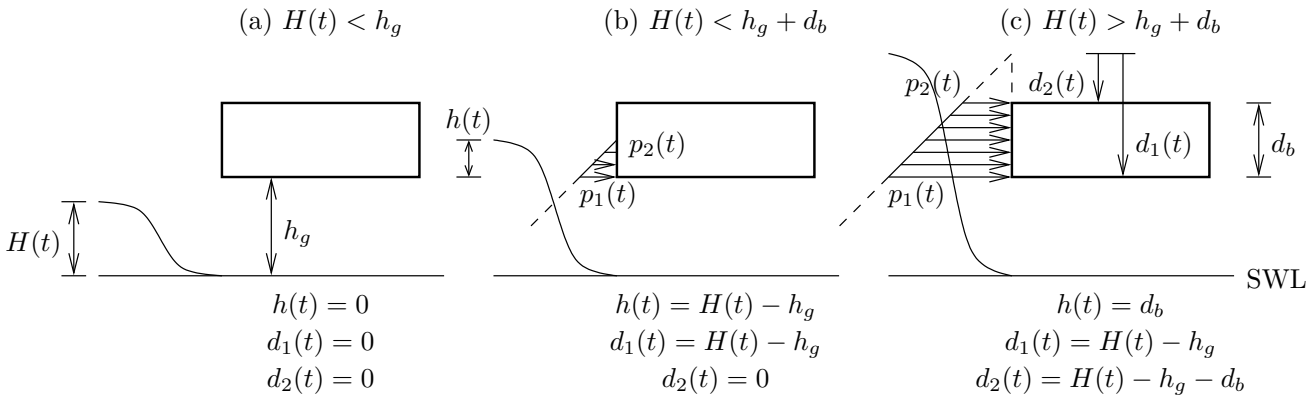

Figure 3.3: Flow height across object for hydrostatic force calculation: (a) flow below object; (b) flow on object; and (c) flow above object.

Given flow conditions, i.e., time histories of wave height, $H(t)$, and wave speed, $u(t)$, from wave flume experiments or from probabilistic tsunami hazard analysis, time histories of hydrodynamic and hydrostatic forces from equations (3.4) and (3.5), respectively, can be computed then combined via equation (3.3) as total force acting on the mass-spring-damper system shown in figure 3.1.

3.2 Description of Experiments

After the 2011 Tohoku earthquake and tsunami, the Public Works Research Institute (PWRI) in Japan conducted a series of wave flume experiments on 1:20 length scale bridge superstructure models for various wave heights. A tsunami bore is generated by release of the gate which holds a reservoir of water. The reservoir depth and standing water level in the flume are adjusted in order to generate an expected wave height. Two wave gauges are located 1.0 m and 2.5 m upstream from the model bridge in order to measure the approaching wave height. In addition, to measure the wave speed, a velocity gauge is located 0.05 m (5 cm) above the flume floor, also 1.0 m upstream from the model bridge. All bridge models, constructed of plywood, were 0.985 m wide, essentially covering

the entire 1.0 m width of the wave flume, and were attached to a fixed pier 20 cm above the flume floor. Additional details on the PWRI experimental setup can be found in [3] and [14].

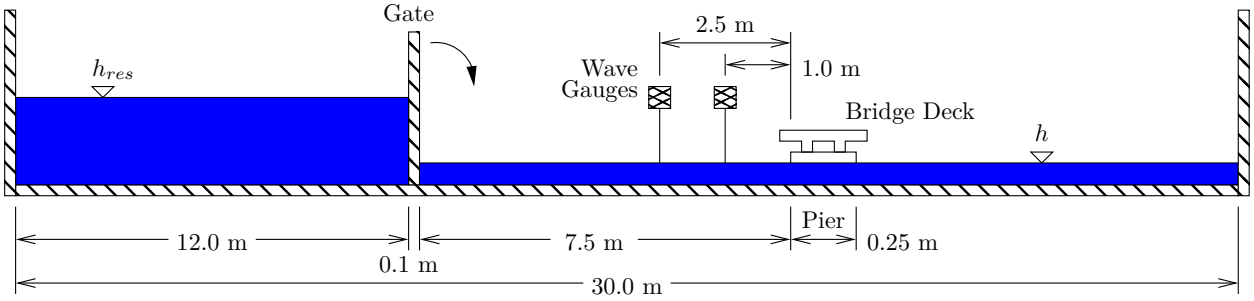

Figure 3.4: Dimensions of wave flume experiments conducted at PWRI.

3.3 Loading Histories

Using the wave height and speed recorded in the PWRI experiments, four loading histories will be developed and applied to the SDF model, then compared with experimentally recorded reaction forces. The loading histories are based on the combination of hydrostatic and hydrodynamic forces shown in equation (3.3) using the following scenarios:

1. $H(t)$ and $u(t)$ – the recorded wave height and wave speed
2. u_{max} and H at u_{max} – the maximum wave speed and the coincident wave height
3. H_{max} and u at H_{max} – the maximum wave height and the coincident wave speed
4. H_{max} and u_{max} – the maximum wave height and the maximum wave speed; Note that these two maxima do not necessarily occur at the same time

It is expected that the three loading scenarios based on maxima of wave height and speed will give more conservative estimates of horizontal force than the scenario based on the time varying wave height and speed.

4 Slab Bridge

The first bridge model for which experimental data was made available is the slab bridge shown in figure 4.1, which is representative of box girder and closed soffit bridges. At model scale, the bridge is 5 cm tall and 25 cm wide, translating to a 1.0 m tall by 5.0 m wide bridge superstructure at prototype scale. Assuming the density of plywood to be 600 kg/m^3, the mass of the slab bridge at prototype scale is m=59,100 kg.

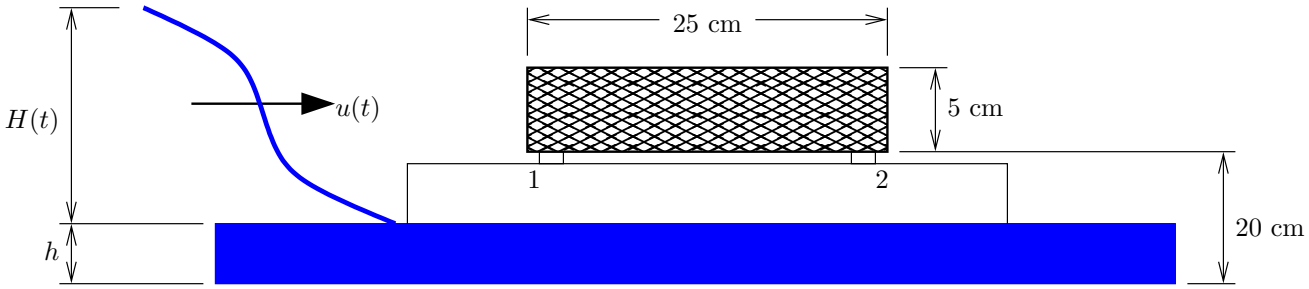

Figure 4.1: Model dimensions for slab bridge in PWRI wave flume experiments.

The bridge is supported at the two locations numbered 1 and 2 in figure 4.1, where load cells were placed in order to record the reaction force history. Using the recordings of wave height and speed, the simulated horizontal reaction force history from the simplified mass-spring-damper system is compared to the experimentally observed forces for five cases of clearance and wave height, as shown in the following sections.

4.1 2 m Clearance, 4 m Wave Height

The first case considered has a standing water level of 10 cm, giving 10 cm clearance (2 m at prototype scale), and expected wave height of 20 cm (4 m at prototype scale). This wave height is sufficient to overtop the model bridge, which is confirmed by the time history of wave height exceeding 3 m, as shown in figure 4.2 (a). The peak wave speed shown in figure 4.2 (b) is over 7 m/s. The forcing function developed from the histories of wave height and speed, along with the three forcing functions based on the maxima of wave height and speed are shown in figure 4.2 (c).

Using the simplified mass-spring-damper analytical model with forcing function, the simulated total horizontal force over-estimates the peak experimental observation as well as the post-peak steady state response (figure 4.3 (a)). Likewise, as shown in figure 4.3 (b), the simulated responses based on maxima of wave height and speed also over-estimate the peak horizontal force. Note that the simulated responses shown in figure 4.3 are computed assuming T_n=0.02 sec for the simplified analytical model, i.e., essentially a rigid connection between the slab bridge and its substructure. The dependence of the peak horizontal force as the natural period increases, e.g., due to an increase in mass or reduction of stiffness in the substructure connection is shown in figure 4.4, where it is observed that the peak force generally increases with the natural period.

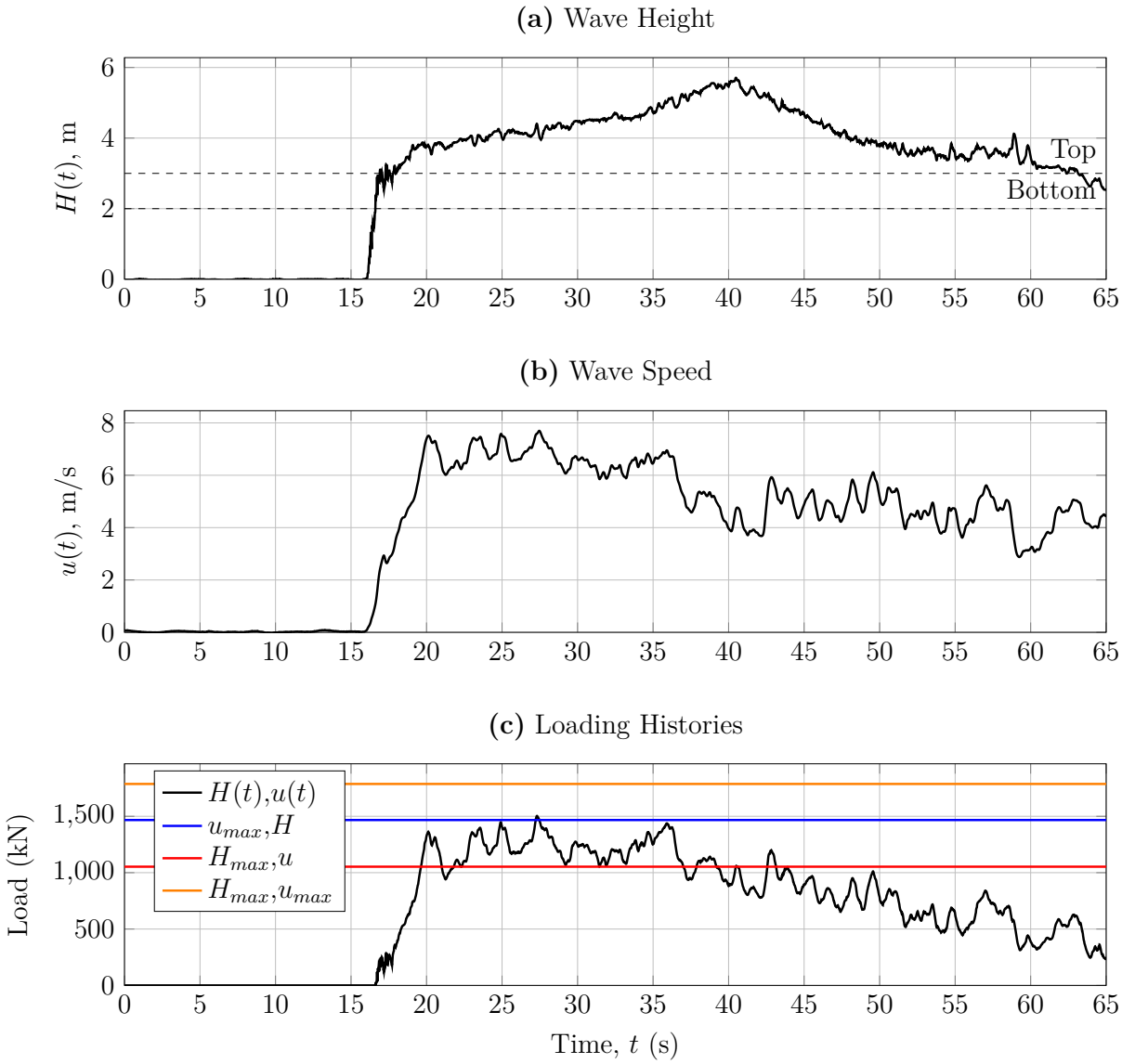

Figure 4.2: Slab bridge with 2 m clearance and 4 m wave height: (a) time history of wave height; (b) time history of wave speed; (c) time history of loading and loadings based on maxima of wave height and speed.

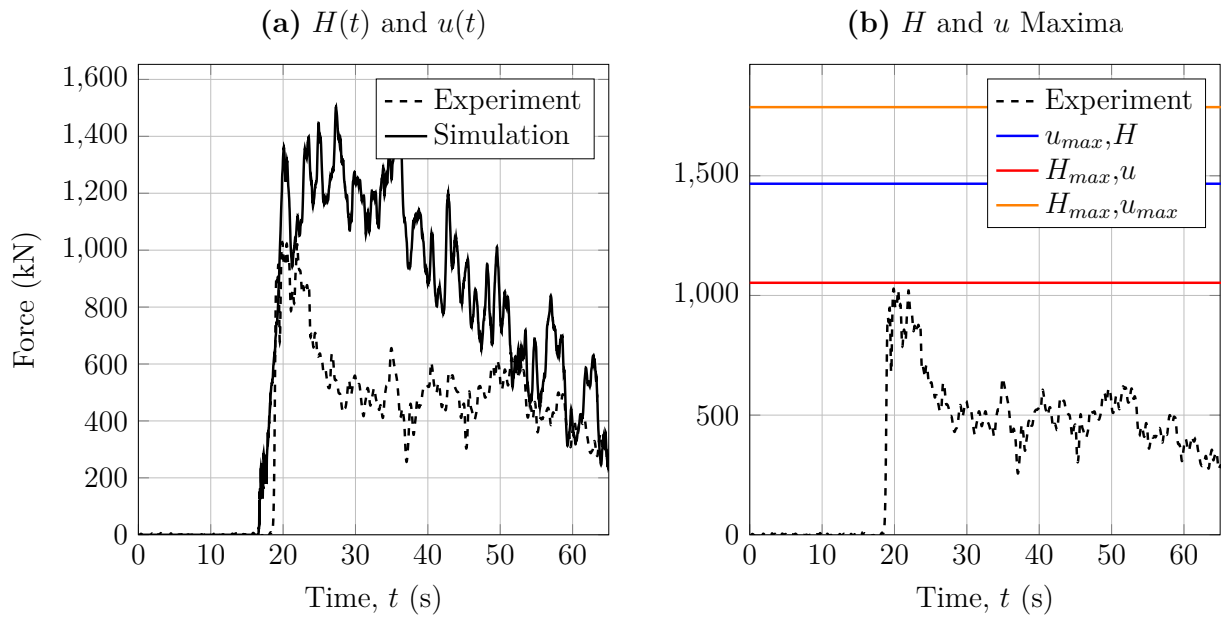

Figure 4.3: Slab bridge with 2 m clearance and 4 m wave height: (a) comparison of experimental and simulated reaction forces and (b) comparison of experimental and maxima-based reaction forces.

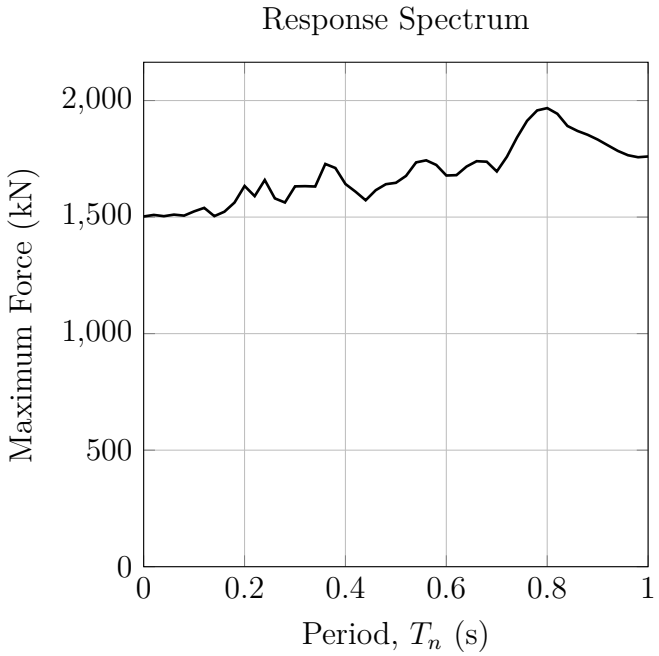

Figure 4.4: Slab bridge with 2 m clearance and 4 m wave height: response spectrum for maximum horizontal force based on time histories of wave height and speed and 5% structural damping.

4.2 1 m Clearance, 2 m Wave Height

The second case has standing water level of 15 cm (1 m clearance at prototype scale) and expected wave height of 10 cm (2 m at prototype scale). This wave height should just reach the top of the model bridge, i.e., the maximum wave height is 2 m, as shown in figure 4.5 (a). The peak wave speed shown in figure 4.5 (b) is approximately 4 m/s; however, this peak occurs well after first impact, at which point the peak speed is approximately 3 m/s. The forcing function developed from the histories of wave height and speed, along with the three forcing functions based on the maxima of wave height and speed are shown in figure 4.5 (c).

As shown in figure 4.6 (a), the simulated total horizontal force (assuming T_n=0.02 sec) is not able to capture the large impact force recorded in the experiment. However, the simulation captures the early stages of transient response, but on the other hand it over-predicts the steady state response. figure 4.6 (b) shows that the simulated responses using the maxima of wave height and speed approach the recorded peak horizontal force; however, this is coincidental because the large peak is likely due to other effects, e.g., pressure shocks, not taken in to account with the simplified model As the natural period of the system increases, there is a significant increase in the peak horizontal force shown in the response spectrum of figure 4.7.

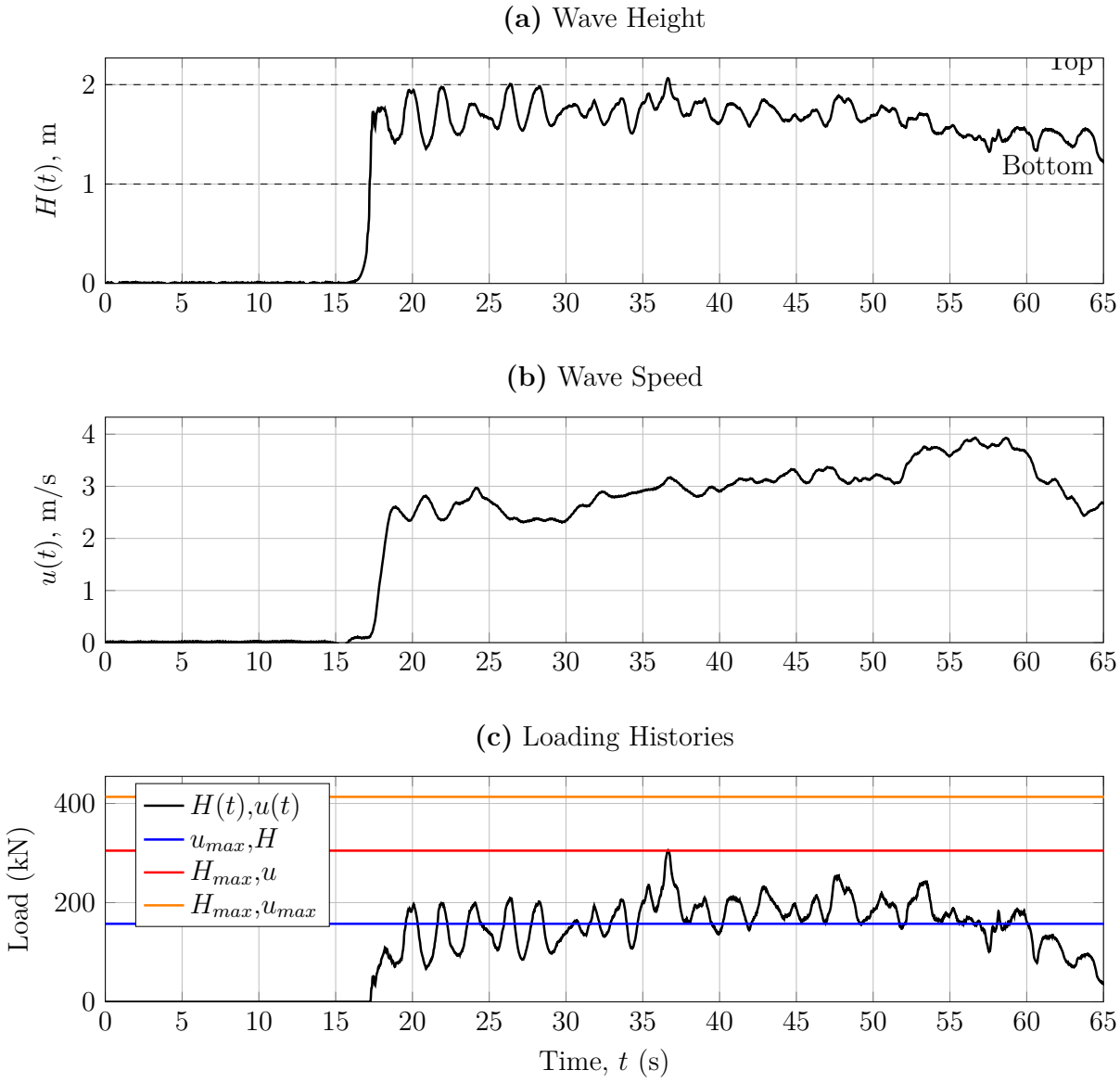

Figure 4.5: Slab bridge model with 1 m clearance and 2 m wave height: (a) time history of wave height; (b) time history of wave speed; (c) time history of loading and loadings based on maxima of wave height and speed.

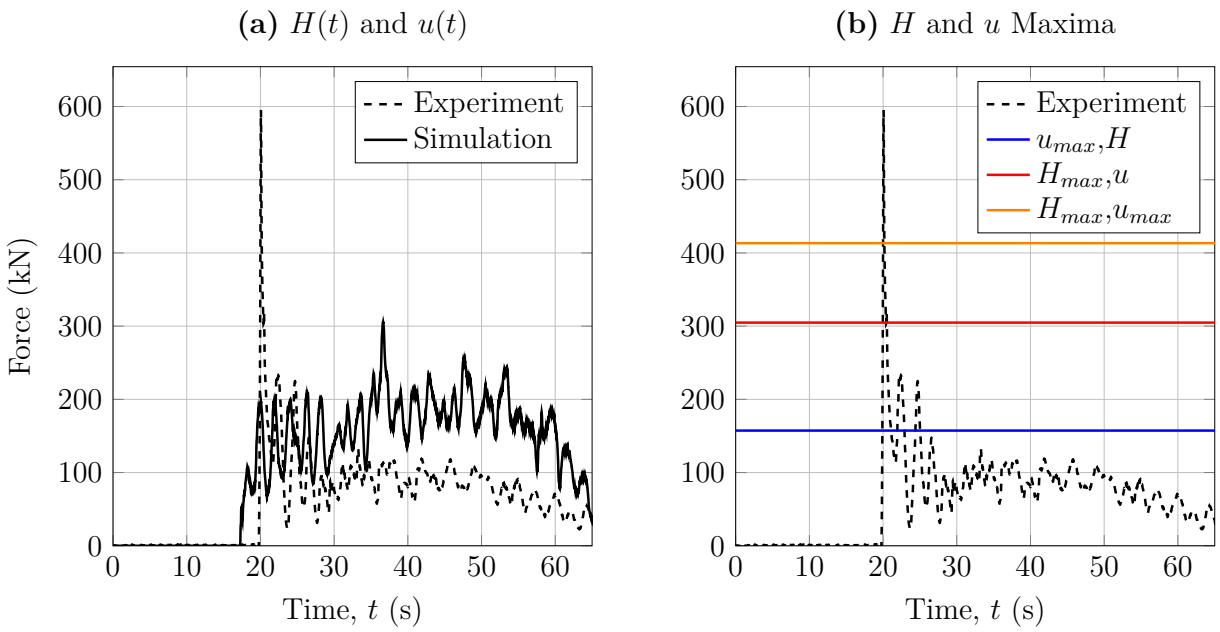

Figure 4.6: Slab bridge model with 1 m clearance and 2 m wave height: (a) comparison of experimental and simulated reaction forces and (b) comparison of experimental and maxima-based reaction forces.

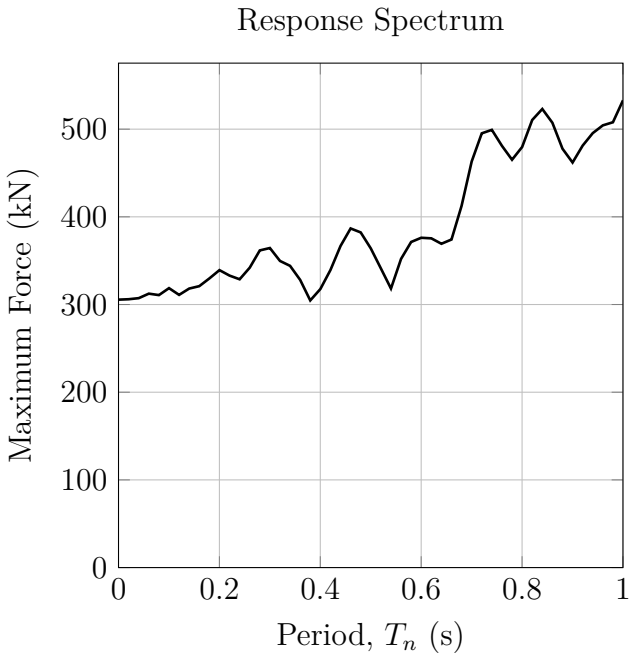

Figure 4.7: Slab bridge model with 1 m clearance and 2 m wave height: response spectrum for maximum horizontal force based on time histories of wave height and speed and 5% structural damping.

4.3 1 m Clearance, 3 m Wave Height

In the third case, the standing water level is 15 cm (1 m clearance at prototype scale) and the expected wave height is 15 cm (3 m prototype), which is sufficient to overtop the model bridge. As shown in figure 4.8 (a), the wave reaches its expected height, while in figure 4.8 (b) the peak speed is just under 5 m/s. The forcing function developed from the histories of wave height and speed, along with the three forcing functions based on the maxima of wave height and speed are shown in figure 4.8 (c).

As in the previous case, the simplified simulation is not able to capture the large impact force observed in the experiments; however, there is good agreement of the steady state response in figure 4.9 (a). Discrepancies arise in the steady state response as the simulated force decreases significantly after time of 50 sec. There is little variance in the simulated responses based on maxima of wave height and speed (figure 4.9 (b)) because the recorded wave height and speed remain fairly uniform through the experiment. As shown in figure 4.10, there is very little dependence of the maximum horizontal force on the natural period of the bridge superstructure.

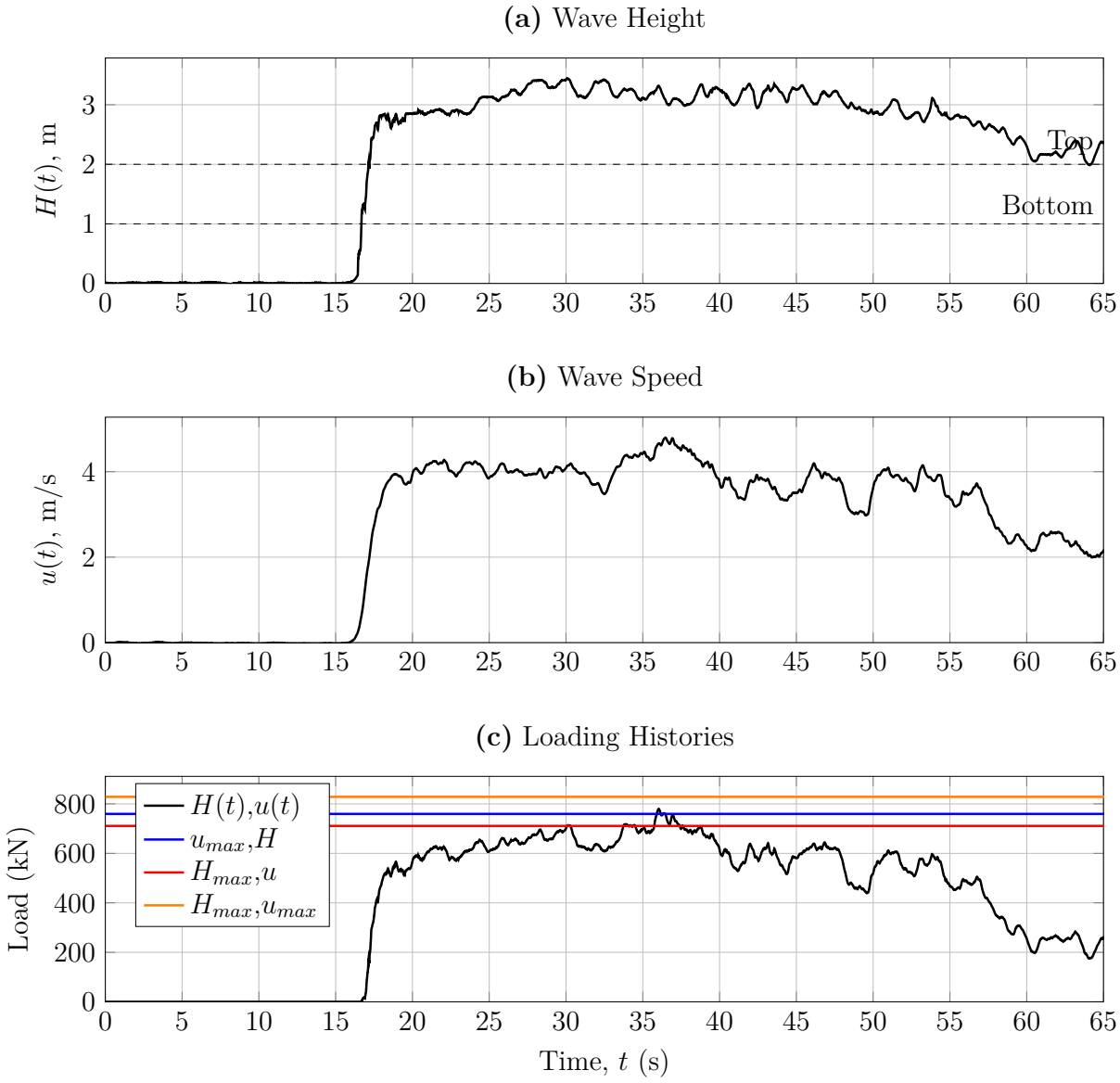

Figure 4.8: Slab bridge with 1 m clearance and 3 m wave height: at prototype scale: (a) time history of wave height; (b) time history of wave speed; (c) time history of loading and loadings based on maxima of wave height and speed.

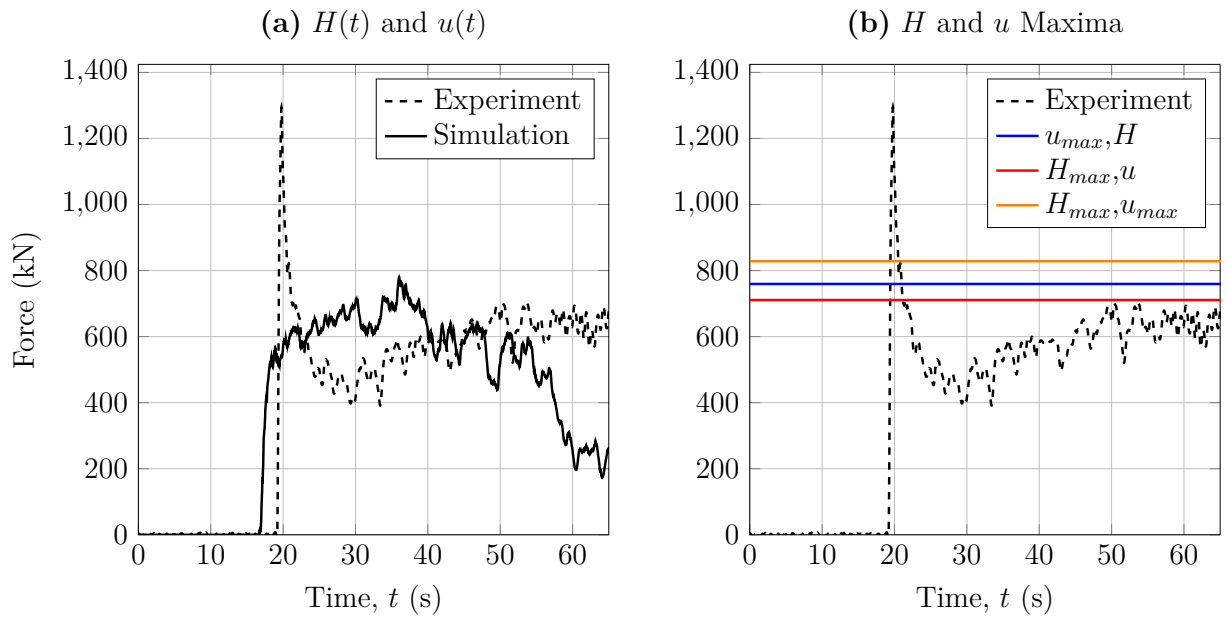

Figure 4.9: Slab bridge with 1 m clearance and 3 m wave height: (a) comparison of experimental and simulated reaction forces and (b) comparison of experimental and maxima-based reaction forces.

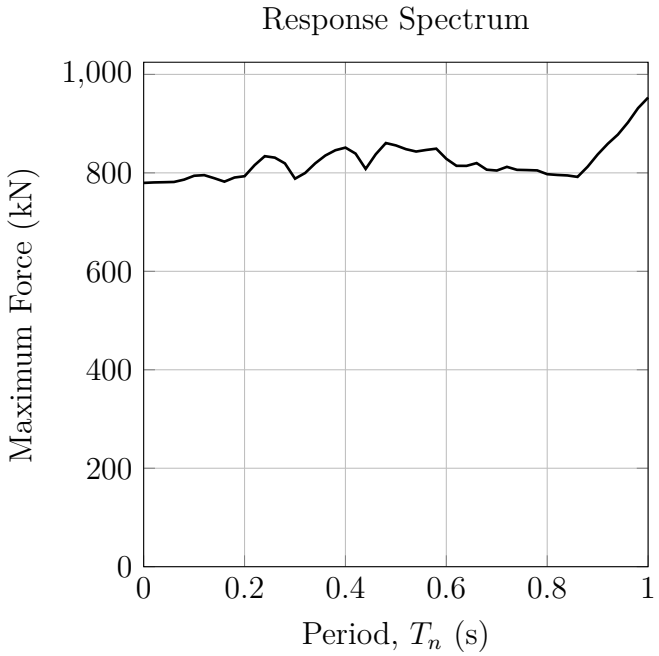

Figure 4.10: Slab bridge with 1 m clearance and 3 m wave height: response spectrum for maximum horizontal force based on time histories of wave height and speed and 5% structural damping.

4.4 No Clearance, 2 m Wave Height

For the fourth case, the standing water level is 20 cm, giving no clearance, i.e., the standing water is at the underside of the model bridge. The expected wave height is 10 cm (2 m at prototype scale) will overtop the model bridge. After some initial oscillations observed in figure 4.11 (a), the wave reaches its expected height and the peak wave speed is over 3 m/s as shown in figure 4.11 (b). The forcing function developed from the histories of wave height and speed, along with the three forcing functions based on the maxima of wave height and speed are shown in figure 4.11 (c).

Although the simplified simulation under predicts the initial peaks of total horizontal force, it captures the basic trends and reasonably reproduces the steady state response, as shown in figure 4.12 (a). The simulated responses based on maxima of wave height and speed are consistent because the peaks of wave height and speed are approximately coincident in the initial stages of wave loading. In addition, the response spectrum shown in figure 4.13 indicates a significant increase in the maximum horizontal force with respect to the natural period of the simplified model. This is due to the oscillatory nature of the large magnitude, initial stages of wave height and speed.

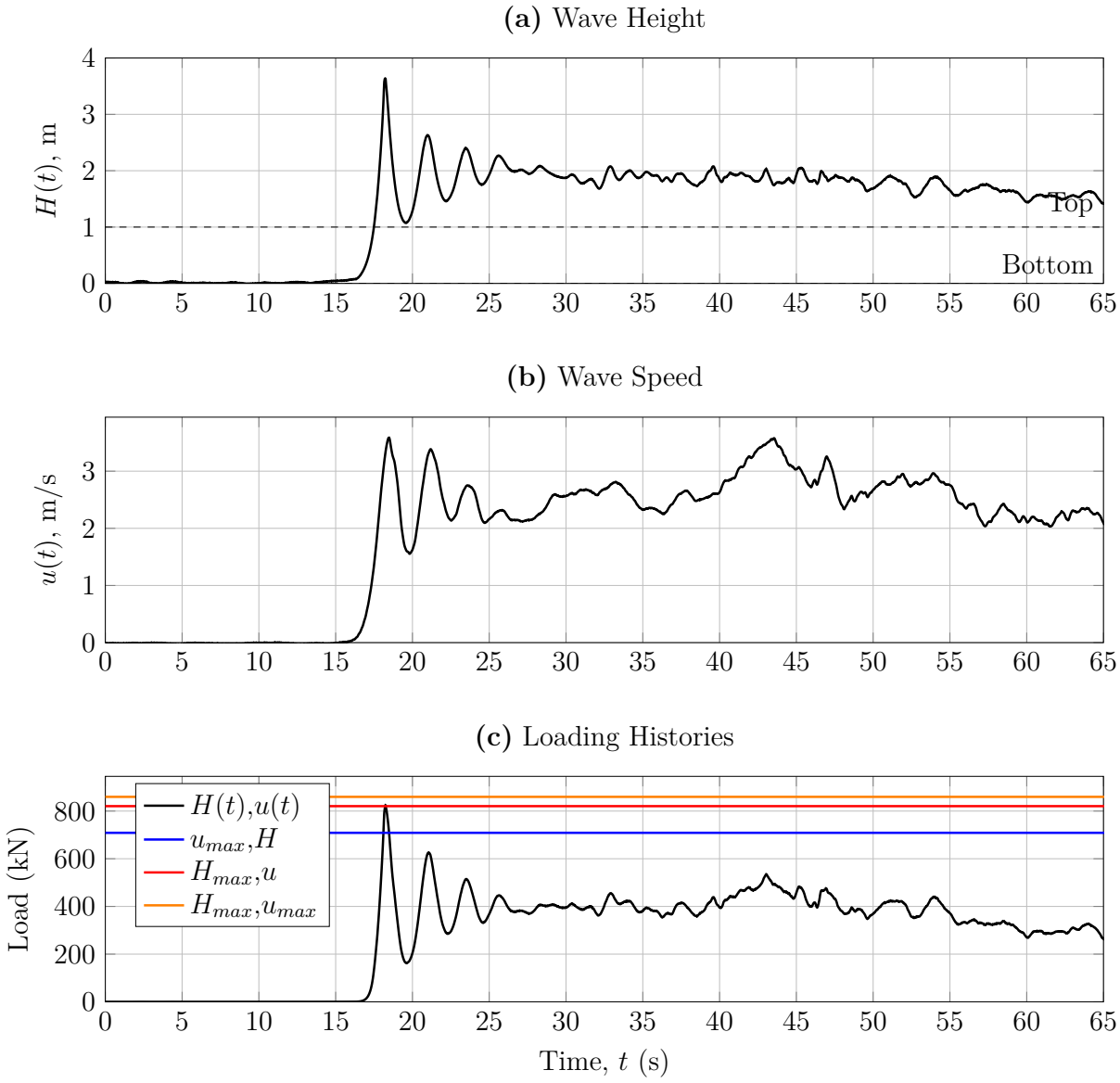

Figure 4.11: Slab bridge with no clearance and 2 m wave height: (a) time history of wave height; (b) time history of wave speed; (c) time history of loading and loadings based on maxima of wave height and speed.

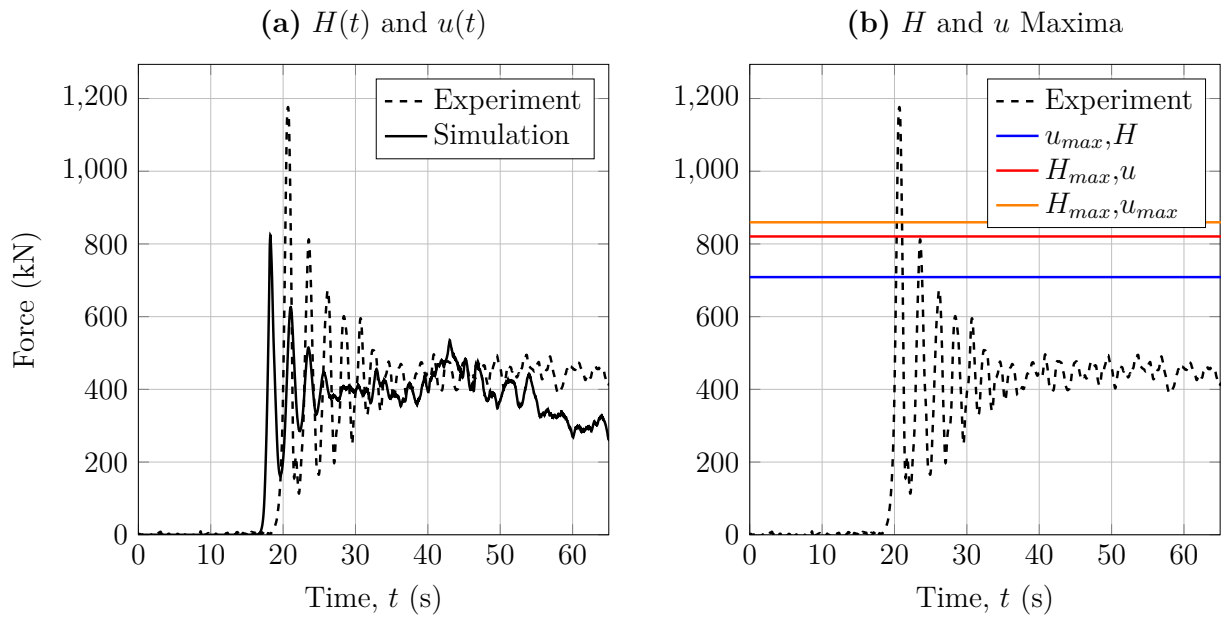

Figure 4.12: Slab bridge with no clearance and 2 m wave height: (a) comparison of experimental and simulated reaction forces and (b) comparison of experimental and maxima-based reaction forces.

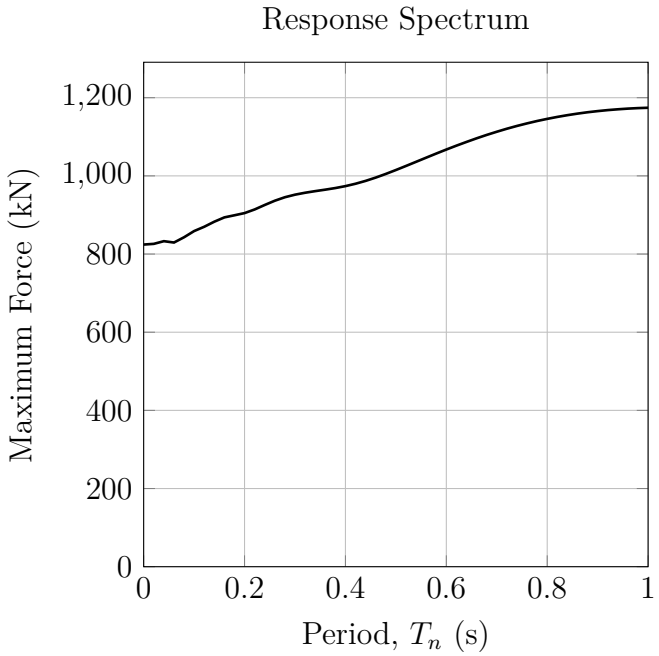

Figure 4.13: Slab bridge with no clearance and 2 m wave height: response spectrum for maximum horizontal force based on time histories of wave height and speed and 5% structural damping.

4.5 No Clearance, 3 m Wave Height

The final case consists of no clearance (20 cm standing water level) and expected wave height of 15 cm (3 m at prototype scale). The expected wave height is sufficient to overtop the model bridge, which is confirmed by the time history shown in figure 4.14 (a). The peak wave speed observed in figure 4.14 (b) is approximately 4 m/s. The forcing function developed from the histories of wave height and speed, along with the three forcing functions based on the maxima of wave height and speed are shown in figure 4.14 (c).

As in previous cases, the simplified simulation is not able to capture the initial spike in horizontal force recorded in the experiment (figure 4.15 (a)). In this case, the simulation generally over-predicts the steady state response. The simulated responses based on maxima of wave height and speed shown in figure 4.15 (b) give similar estimates compared to the loading based on histories of wave height and speed. The response spectrum of figure 4.16 shows very little dependence of the maximum force on the natural period of the model, although there is an increase in maximum force for periods greater than 0.8 sec.

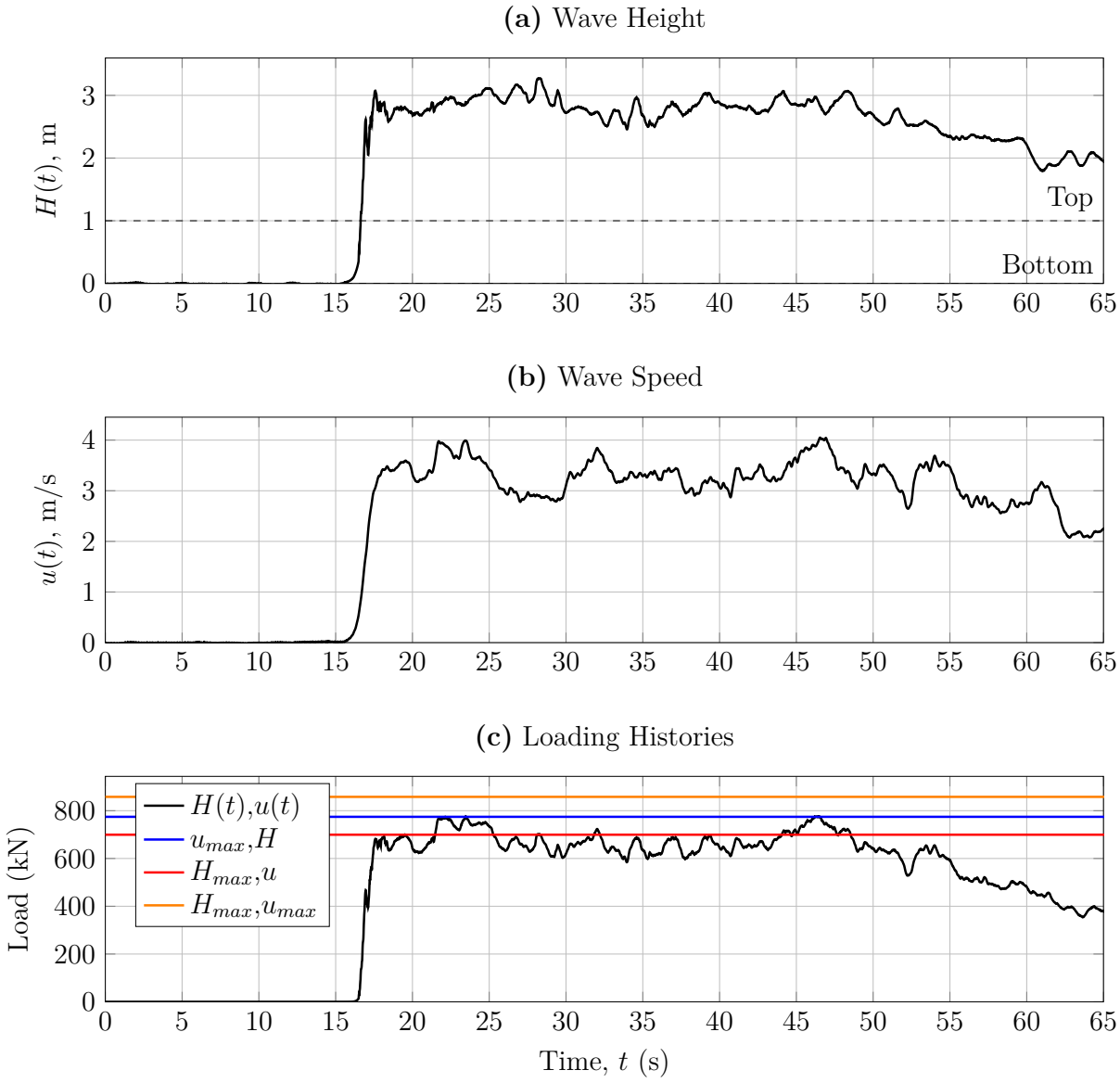

Figure 4.14: Slab bridge with no clearance and 3 m wave height: (a) time history of wave height; (b) time history of wave speed; (c) time history of loading and loadings based on maxima of wave height and speed.

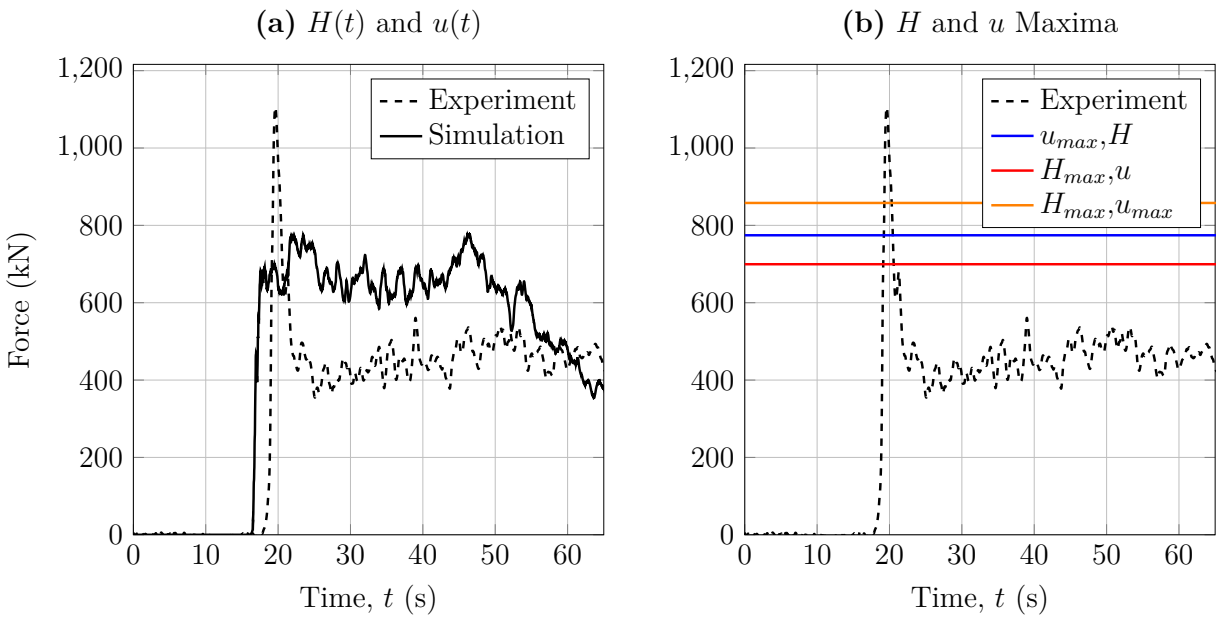

Figure 4.15: Slab bridge with no clearance and 3 m wave height: (a) comparison of experimental and simulated reaction forces and (b) comparison of experimental and maxima-based reaction forces.

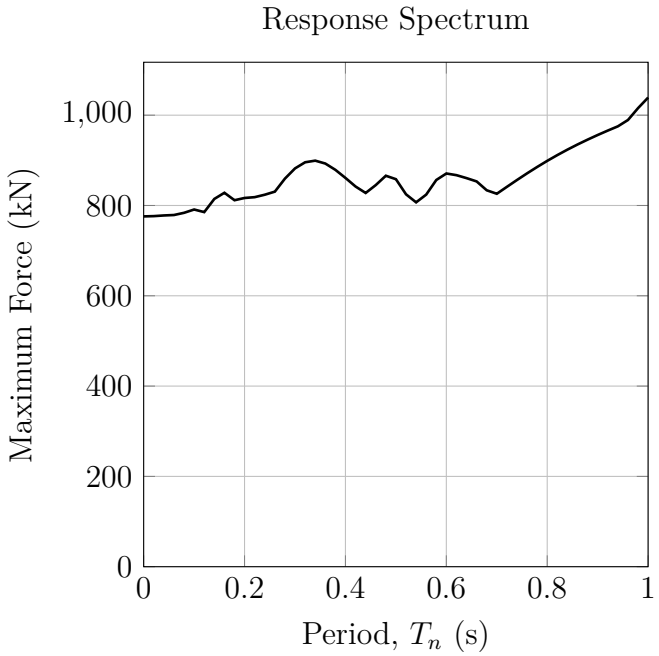

Figure 4.16: Slab bridge with no clearance and 3 m wave height: response spectrum for maximum horizontal force based on time histories of wave height and speed and 5% structural damping.

5 Deck-Girder Bridge

The second bridge model for which experimental data was made available is the deck-girder bridge shown in figure 5.1. At model scale, the bridge is 10 cm tall and 50 cm wide, translating to a 2.0 m tall by 10.0 m wide bridge superstructure at prototype scale. Assuming the density of plywood to be 600 kg/m^3, the mass of the bridge superstructure is m=97,400 kg at prototype scale.

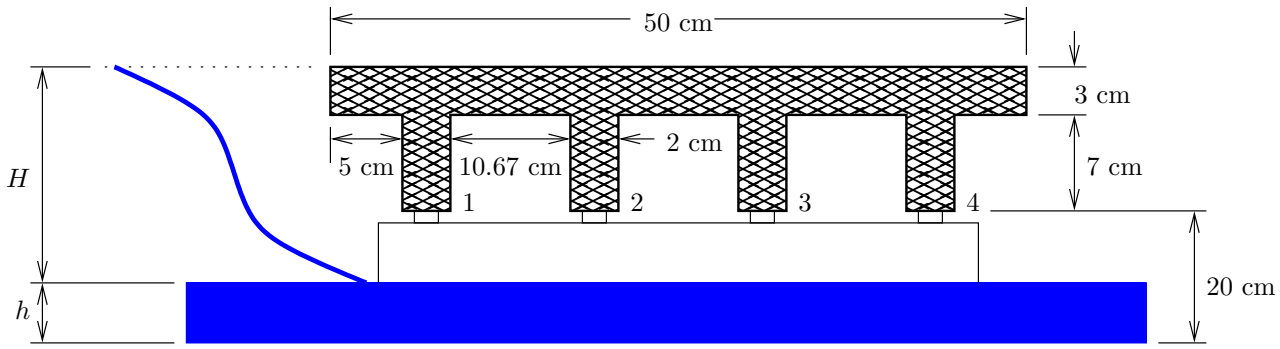

Figure 5.1: Model dimensions for deck-girder bridge in PWRI wave flume experiments.

The bridge is supported at the four locations numbered 1 through 4 in figure 5.1, where load cells were placed in order to record the reaction force history. Using the recordings of wave height and speed, the simulated horizontal reaction force history from the simplified mass-spring-damper system is compared to the experimentally observed forces for five cases of clearance and wave height, as shown in the following sections.

5.1 2 m Clearance, 4 m Wave Height

The first case considered has a standing water level of 10 cm, giving 10 cm clearance (2 m at prototype scale), and expected wave height of 20 cm (4 m at prototype scale). This wave height is sufficient to overtop the model bridge, which is confirmed by the time history of wave height exceeding 4 m, as shown in figure 5.2 (a). The peak wave speed shown in figure 5.2 (b) is over 6 m/s. The forcing function developed from the histories of wave height and speed, along with the three forcing functions based on the maxima of wave height and speed are shown in figure 5.2 (c).

Using the recorded time history of wave height and speed to develop the forcing function for the simplified mass-spring-damper analytical model, the simulated time history of total horizontal force (assuming T_n=0.02 sec) is shown in figure 5.3 (a). Although the peak magnitudes of horizontal force are similar, the simulation misses the initial impact load and tends to over-predict the steady state response. The simulated forces based on maxima of wave height and speed show large variance in figure 5.3 (b). This is due to the large increase in wave height just after 30 sec in the experiment when water starts to build up in front of the bridge, but slows down. Using the simplified model, figure 5.4 shows there is no dependence of the maximum horizontal force on the natural period of the bridge superstructure.

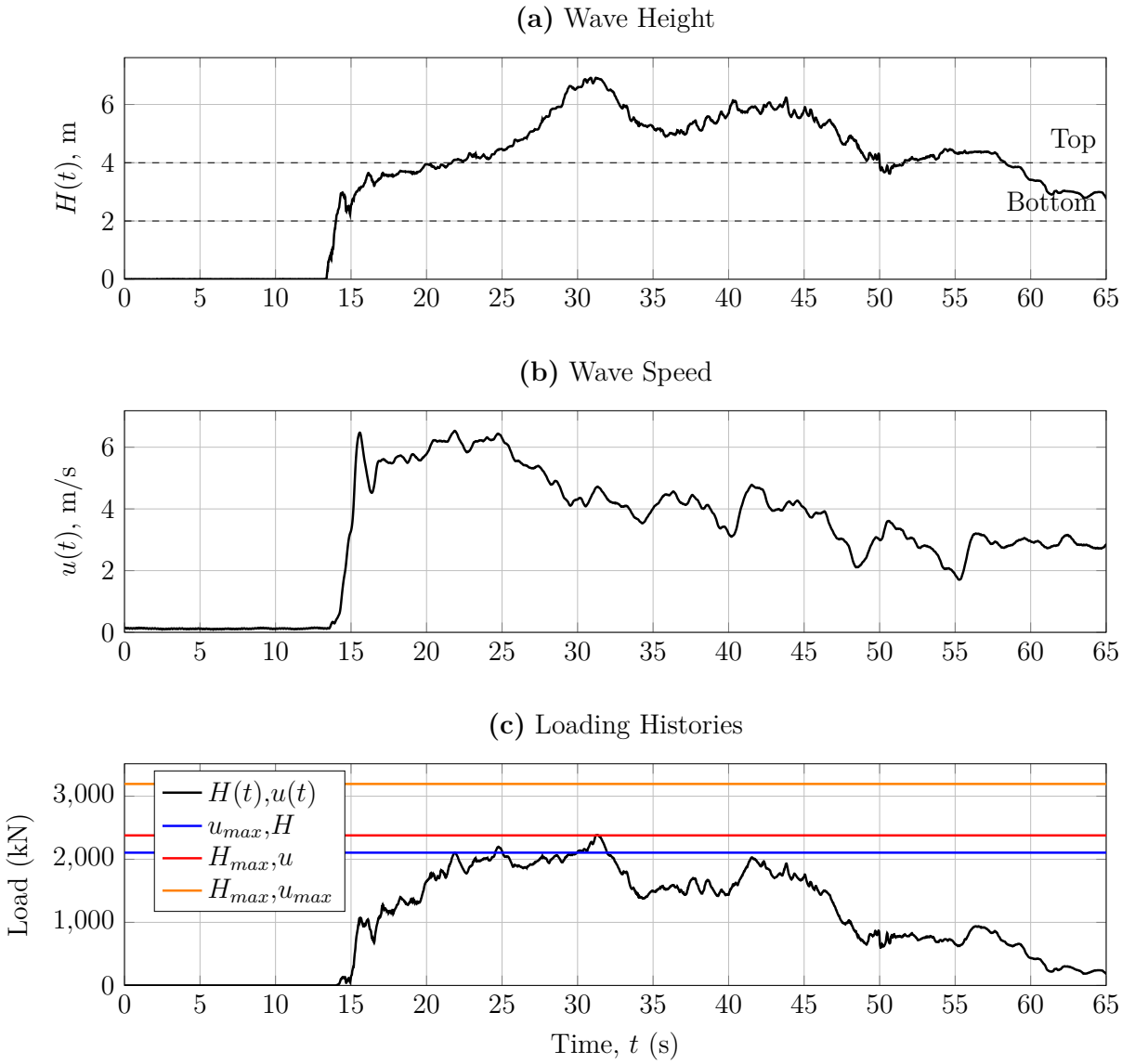

Figure 5.2: Deck-girder bridge with 2 m clearance and 4 m wave height: (a) time history of wave height; (b) time history of wave speed; (c) time history of loading and loadings based on maxima of wave height and speed.

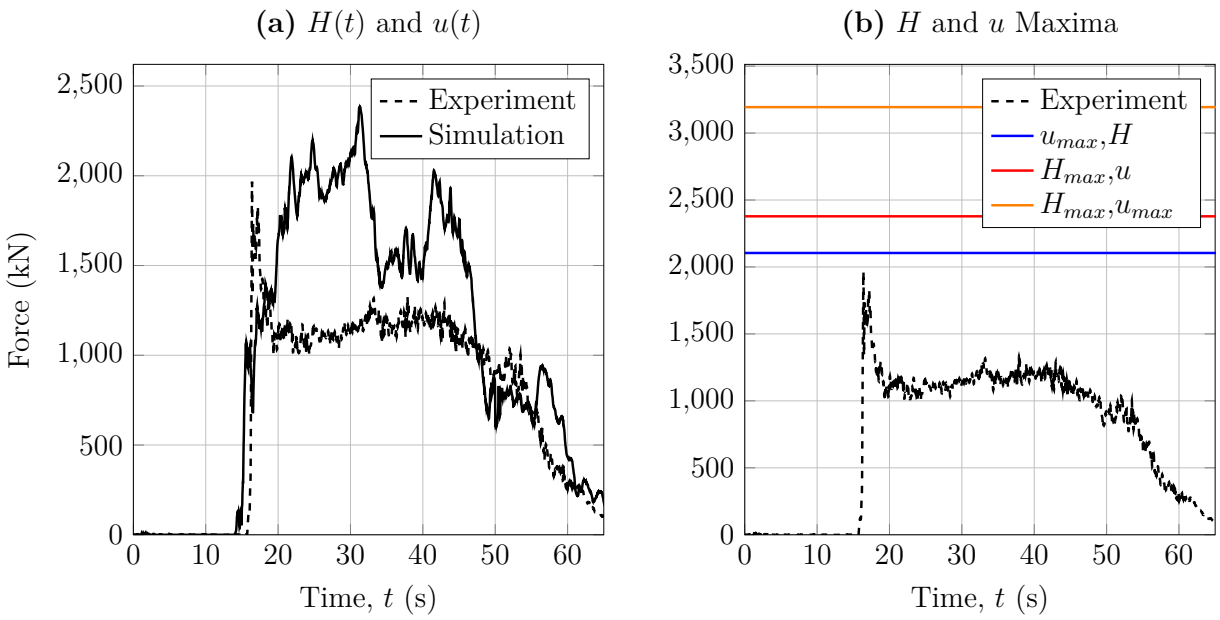

Figure 5.3: Deck-girder bridge with 2 m clearance and 4 m wave height: (a) comparison of experimental and simulated reaction forces and (b) comparison of experimental and maxima-based reaction forces.

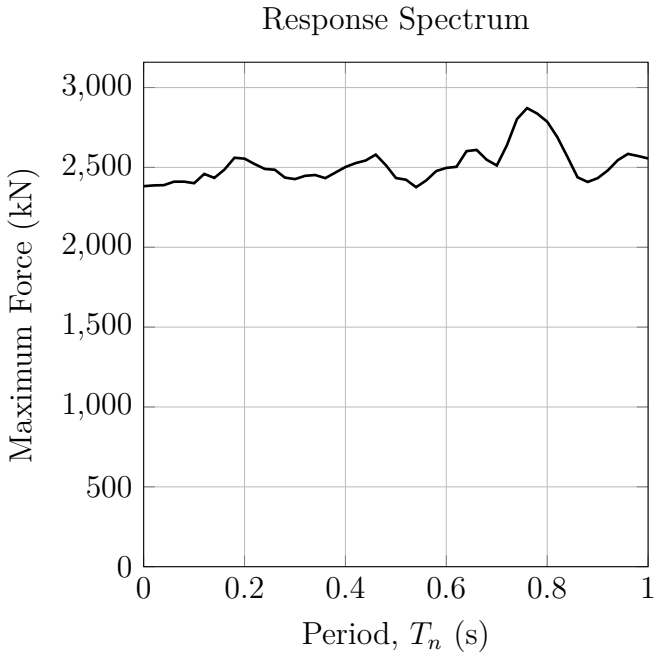

Figure 5.4: Deck-girder bridge with 2 m clearance and 4 m wave height: response spectrum for maximum horizontal force based on time histories of wave height and speed and 5% structural damping.

5.2 1 m Clearance, 2 m Wave Height

The second case has standing water level of 15 cm (1 m clearance at prototype scale) and expected wave height of 10 cm (2 m at prototype scale). This wave height should just reach mid-height of the model bridge, i.e., the maximum wave height is 2 m, as shown in figure 5.5 (a). The peak wave speed shown in figure 5.5 (b) is approximately 3 m/s. The forcing function developed from the histories of wave height and speed, along with the three forcing functions based on the maxima of wave height and speed are shown in figure 5.5 (c).

As shown in figure 5.6 (a), the simplified analytical approach is again not able to capture the initial peak in horizontal force. In addition, it tends to over-predict the steady state response. The maxima of wave height and speed give slightly higher estimates of the horizontal force, but as expected, are also unable to capture the initial peak, which is likely due to pressure shock. There is a general increase in the maximum horizontal force as the natural period of the simplified model increases, as observed in figure 5.7.

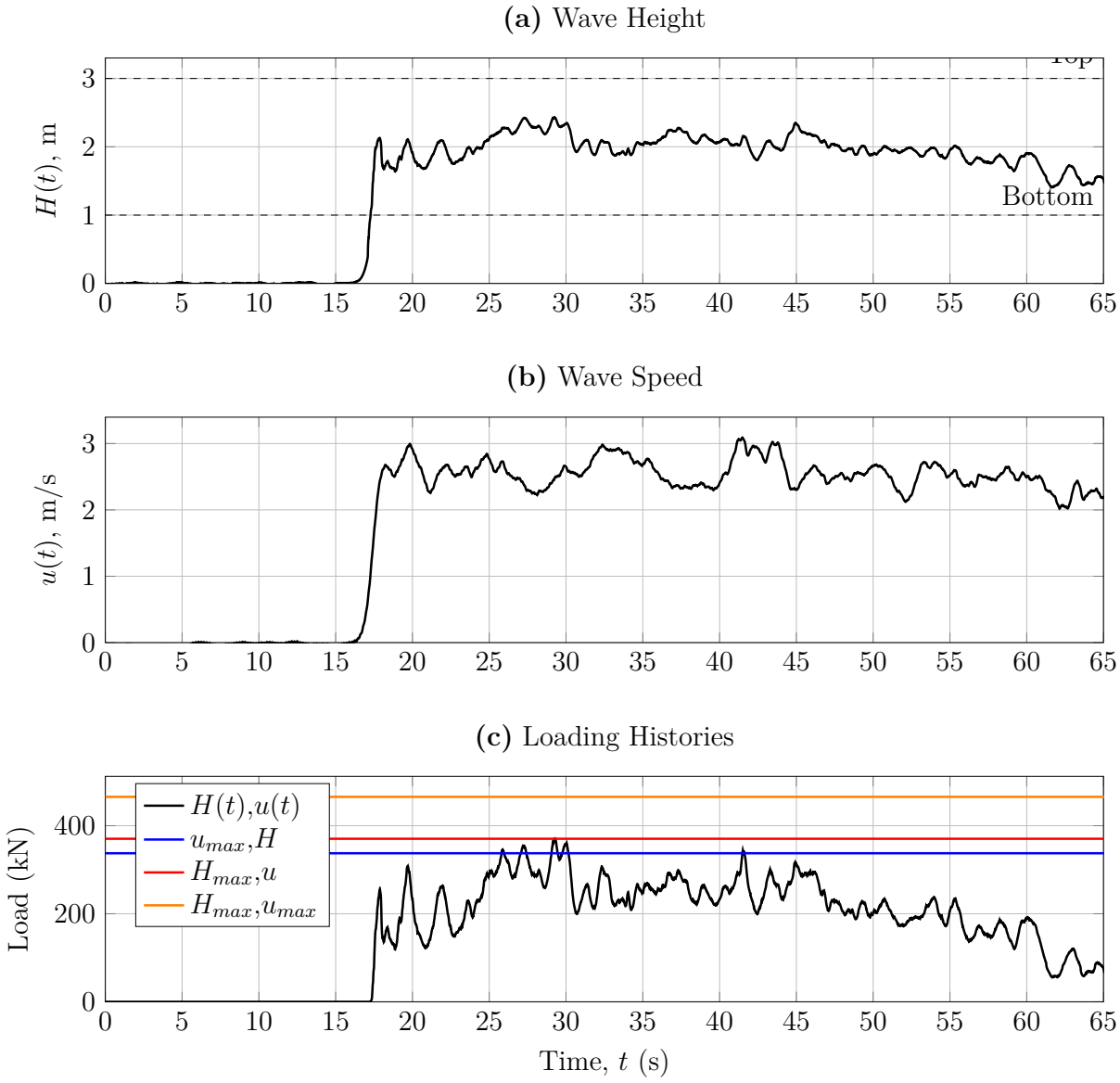

Figure 5.5: Deck-girder bridge with 1 m clearance and 2 m wave height: (a) time history of wave height; (b) time history of wave speed; (c) time history of loading and loadings based on maxima of wave height and speed.

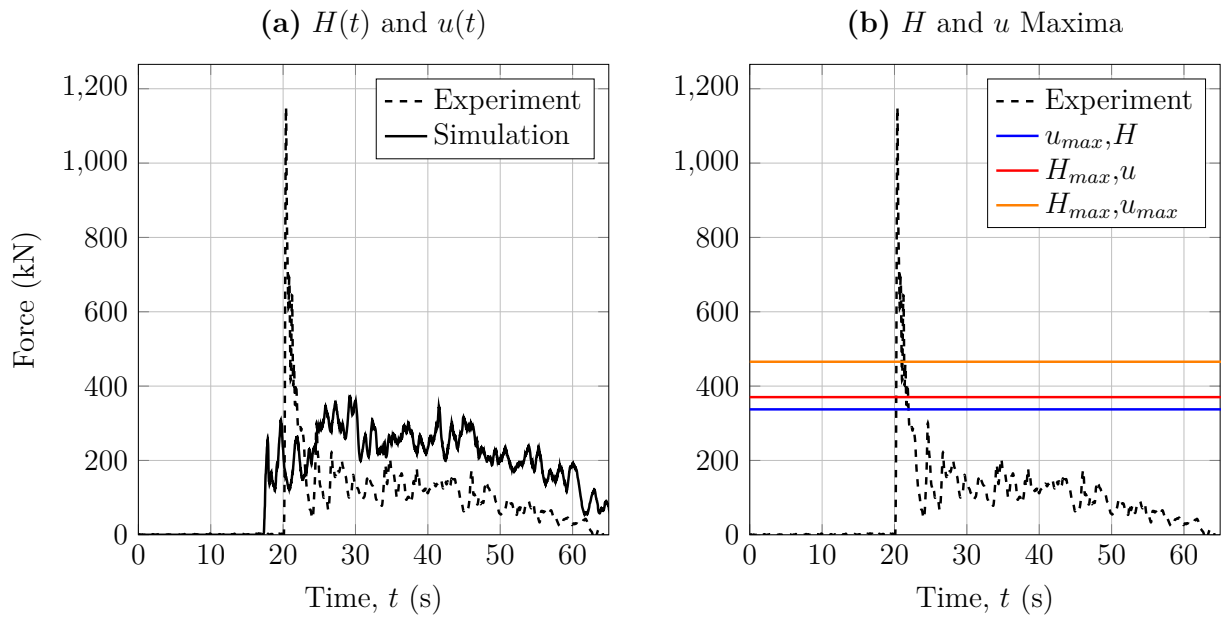

Figure 5.6: Deck-girder bridge with 1 m clearance and 2 m wave height: (a) comparison of experimental and simulated reaction forces and (b) comparison of experimental and maxima-based reaction forces.

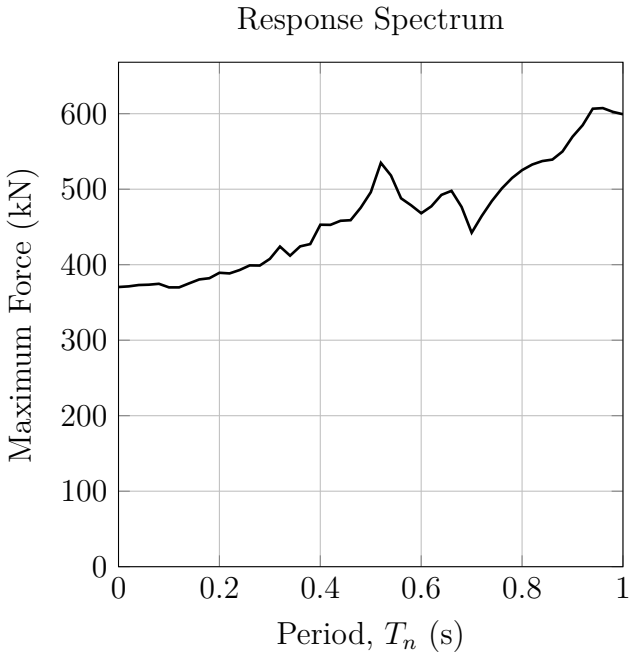

Figure 5.7: Deck-girder bridge with 1 m clearance and 2 m wave height: response spectrum for maximum horizontal force based on time histories of wave height and speed and 5% structural damping.

5.3 1 m Clearance, 3 m Wave Height

In the third case, the standing water level is 15 cm (1 m clearance at prototype scale) and the expected wave height is 15 cm (3 m prototype), which should just reach the top of the model bridge. As shown in figure 5.8 (a), the wave slightly exceeds its expected height by 1 m and overtops the bridge, while in figure 5.8 (b) the peak speed is just about 4 m/s. The forcing function developed from the histories of wave height and speed, along with the three forcing functions based on the maxima of wave height and speed are shown in figure 5.8 (c).

Using the recorded time history of wave height and speed to develop the forcing function for the simplified mass-spring-damper analytical model, the simulated time history of total horizontal force (assuming T_n=0.02 sec) is shown in figure 5.9 (a). The simulation misses the initial impact load and tends to over-predict the steady state response. As shown in figure 5.9 (b), the loading based on H_{max} and u_{max} gives a good estimate of the peak horizontal force, but this is coincidental. For the simplified model, figure 5.10 shows the maximum horizontal force tends to increase as the natural period of the analytical model exceeds 0.5 sec.

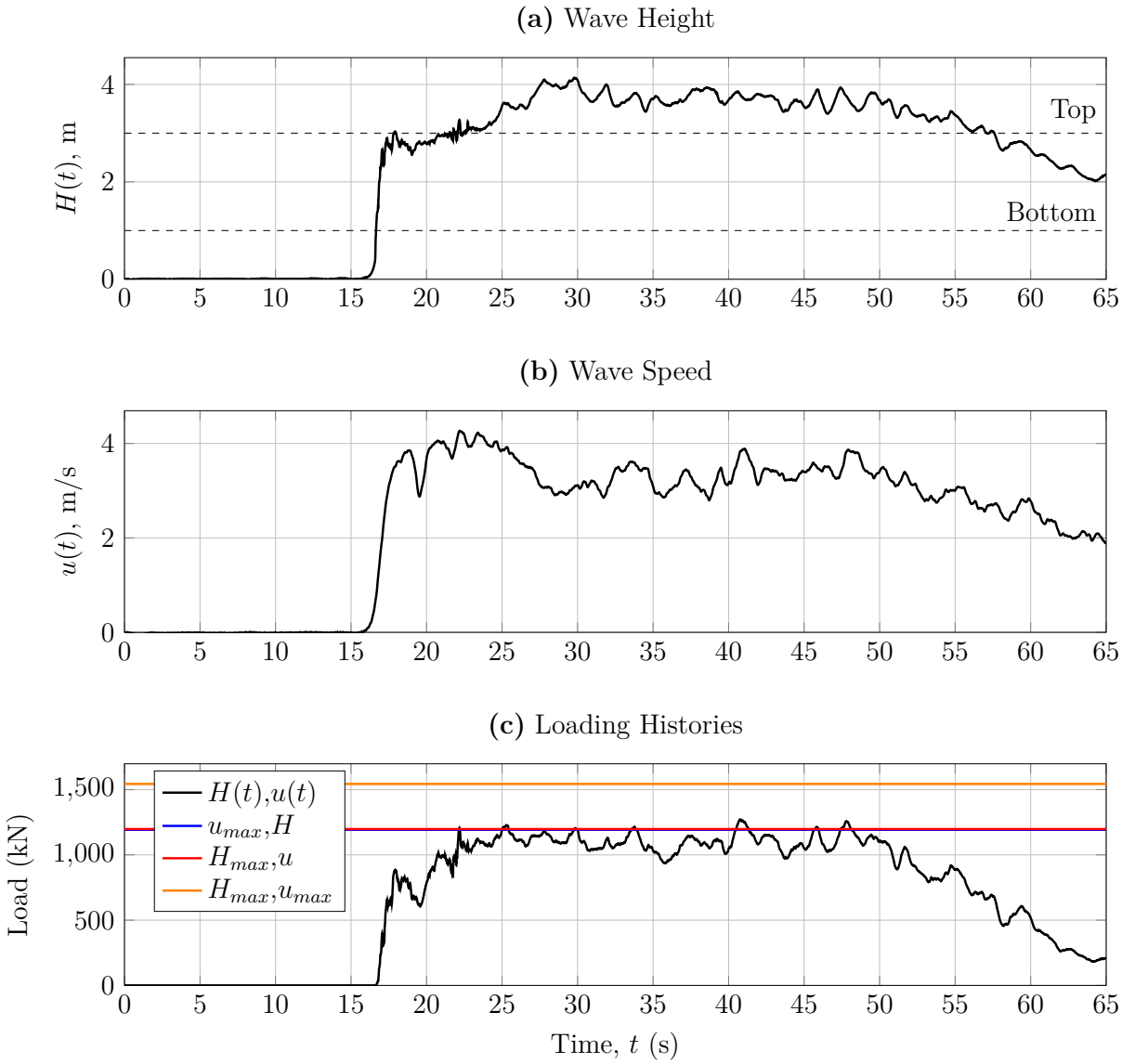

Figure 5.8: Deck-girder bridge with 1 m clearance and 3 m wave height: (a) time history of wave height; (b) time history of wave speed; (c) time history of loading and loadings based on maxima of wave height and speed.

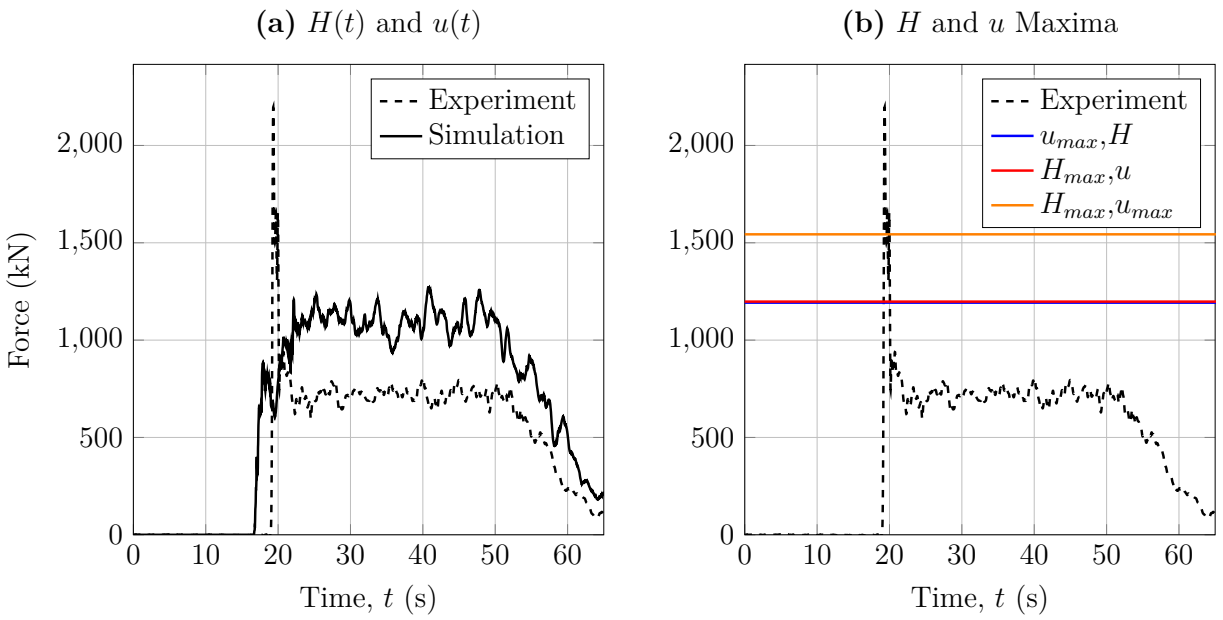

Figure 5.9: Deck-girder bridge with 1 m clearance and 3 m wave height: (a) comparison of experimental and simulated reaction forces and (b) comparison of experimental and maxima-based reaction forces.

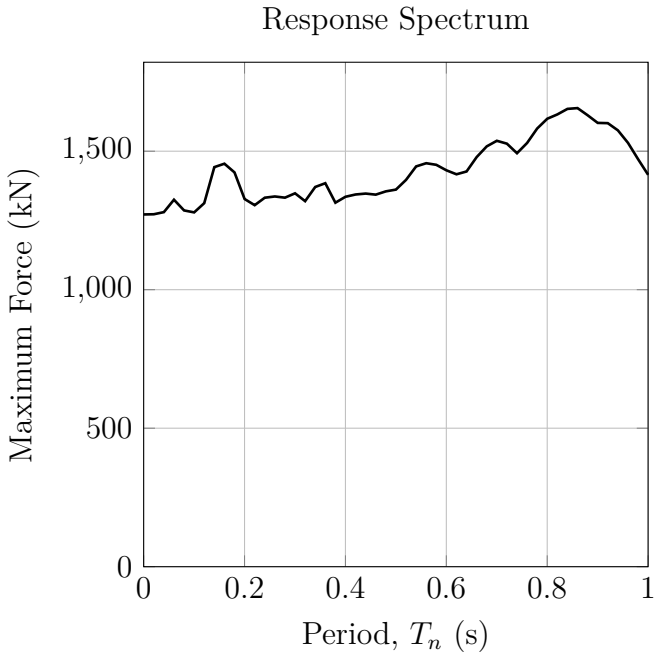

Figure 5.10: Deck-girder bridge with 1 m clearance and 3 m wave height: response spectrum for maximum horizontal force based on time histories of wave height and speed and 5% structural damping.

5.4 No Clearance, 2 m Wave Height

For the fourth case, the standing water level is 20 cm, giving no clearance, i.e., the standing water reaches the underside of the girders in the model bridge. The expected wave height is 10 cm (2 m at prototype scale) will overtop the model bridge. After some initial oscillations observed in figure 5.11 (a), the wave reaches its expected height and the peak wave speed is over 3 m/s as shown in figure 5.11 (b). The forcing function developed from the histories of wave height and speed, along with the three forcing functions based on the maxima of wave height and speed are shown in figure 5.11 (c).

Although the simplified simulation captures the basic trends of oscillation of the horizontal force in the early stages of loading, it generally over predicts the response, as shown in figure 5.12 (a). Similarly, the simulations based on maxima of wave height and speed also over predict the peak response (figure 5.12 (b)). In addition, the response spectrum shown in figure 5.13 indicates a significant increase in the maximum horizontal force with respect to the natural period of the model. This is due to the oscillatory nature of the large magnitude, initial stages of wave height and speed.

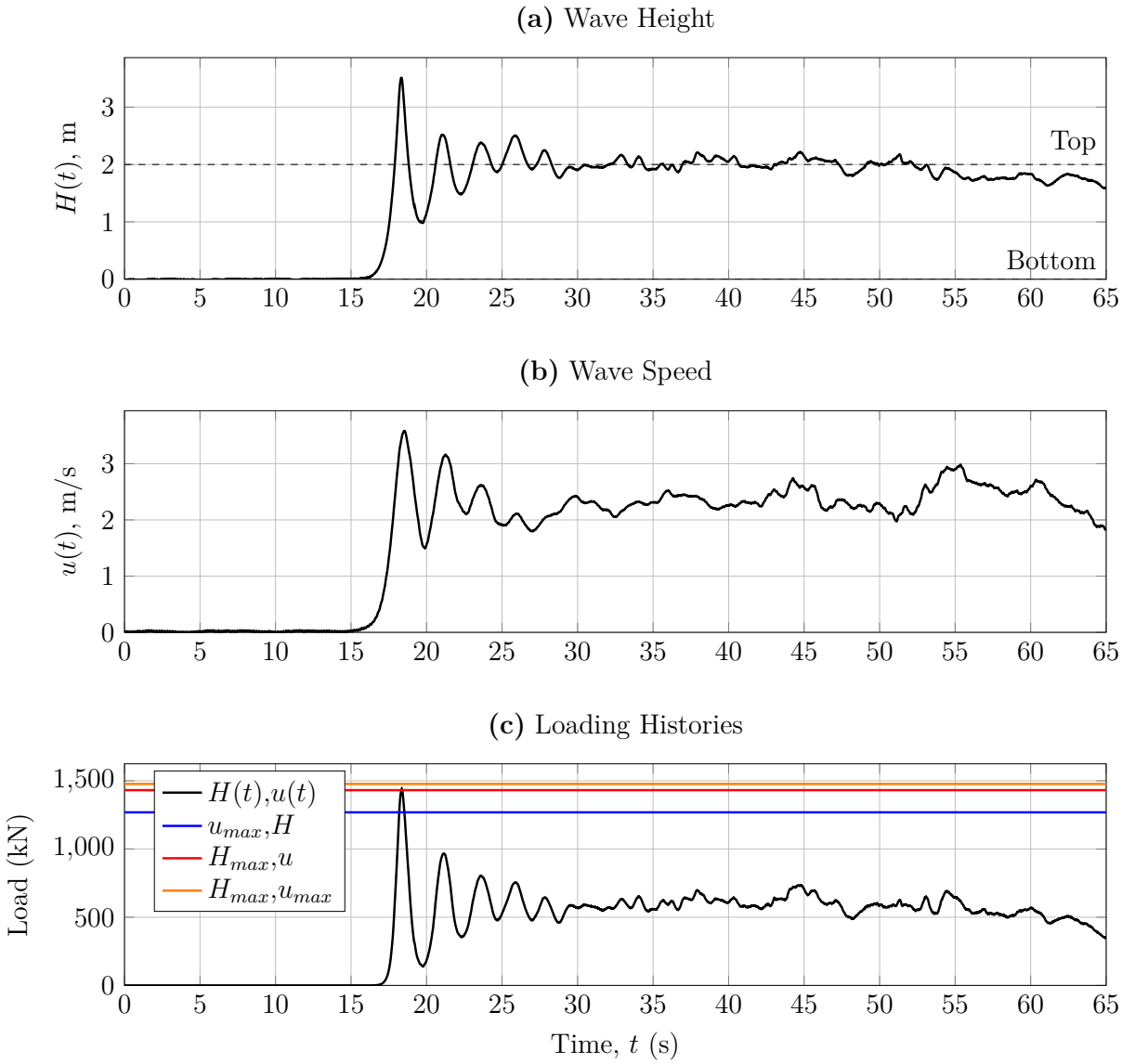

Figure 5.11: Deck-girder bridge with no clearance and 2 m wave height: (a) time history of wave height; (b) time history of wave speed; (c) time history of loading and loadings based on maxima of wave height and speed.

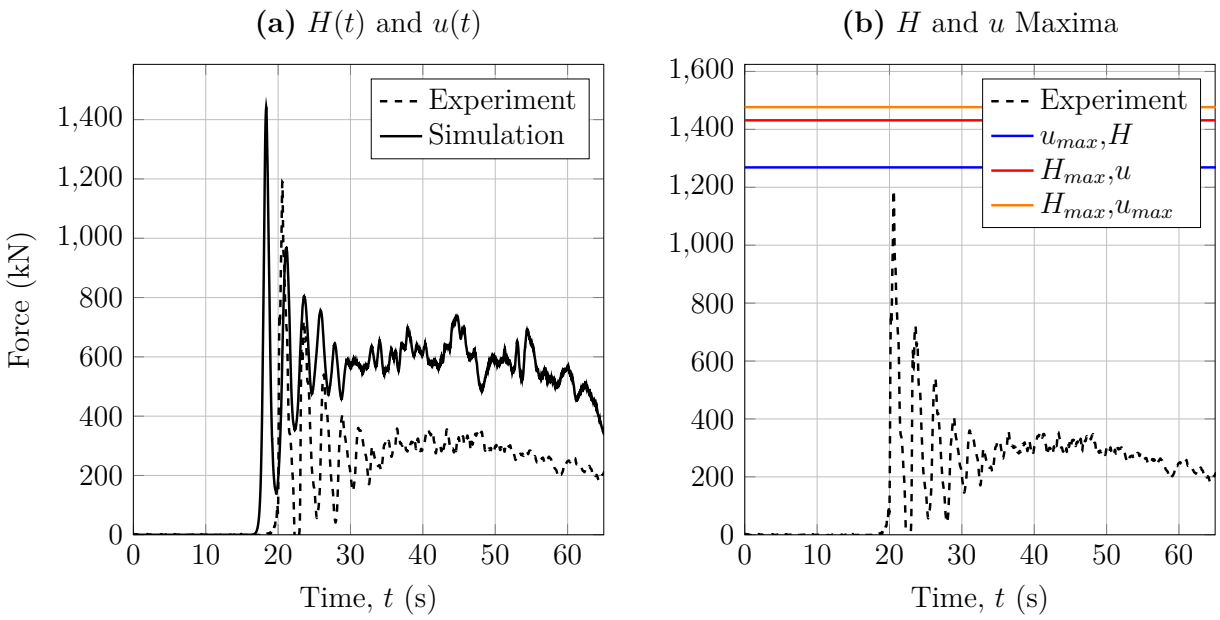

Figure 5.12: Deck-girder bridge with no clearance and 2 m wave height: (a) comparison of experimental and simulated reaction forces and (b) comparison of experimental and maxima-based reaction forces.

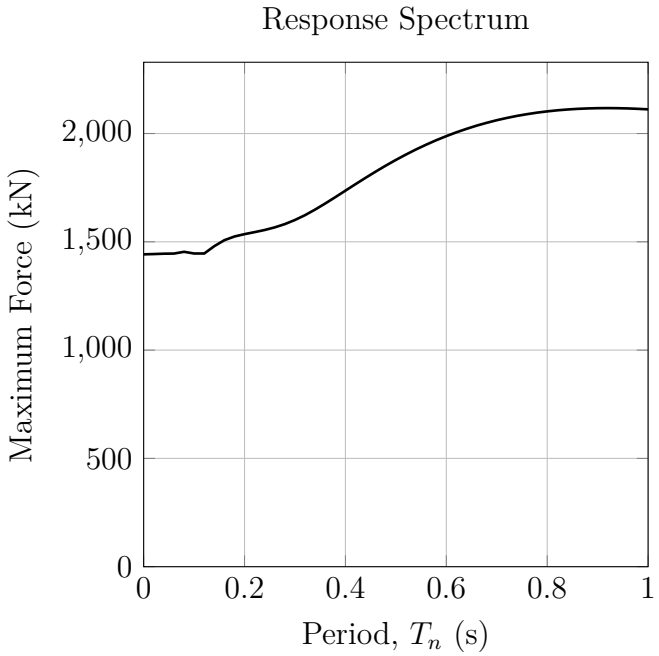

Figure 5.13: Deck-girder bridge with no clearance and 2 m wave height: response spectrum for maximum horizontal force based on time histories of wave height and speed and 5% structural damping.

5.5 No Clearance, 3 m Wave Height

The final case consists of no clearance (20 cm standing water level) and expected wave height of 15 cm (3 m at prototype scale). The expected wave height is sufficient to overtop the bridge, which is confirmed by the time history shown in figure 5.14 (a). The peak wave speed observed in figure 5.14 (b) exceeds 3 m/s. The forcing function developed from the histories of wave height and speed, along with the three forcing functions based on the maxima of wave height and speed are shown in figure 5.14 (c).

As in previous cases, the simplified simulation is not able to capture the initial spike in horizontal force recorded in the experiment (figure 5.15 (a)). In this case, the simulation generally over-predicts the steady state response. The simulated responses based on maxima of wave height and speed give slightly higher peak horizontal force as shown in figure 5.15 (b). The response spectrum of figure 5.16 shows an increase in maximum force for periods greater than 0.4 sec.

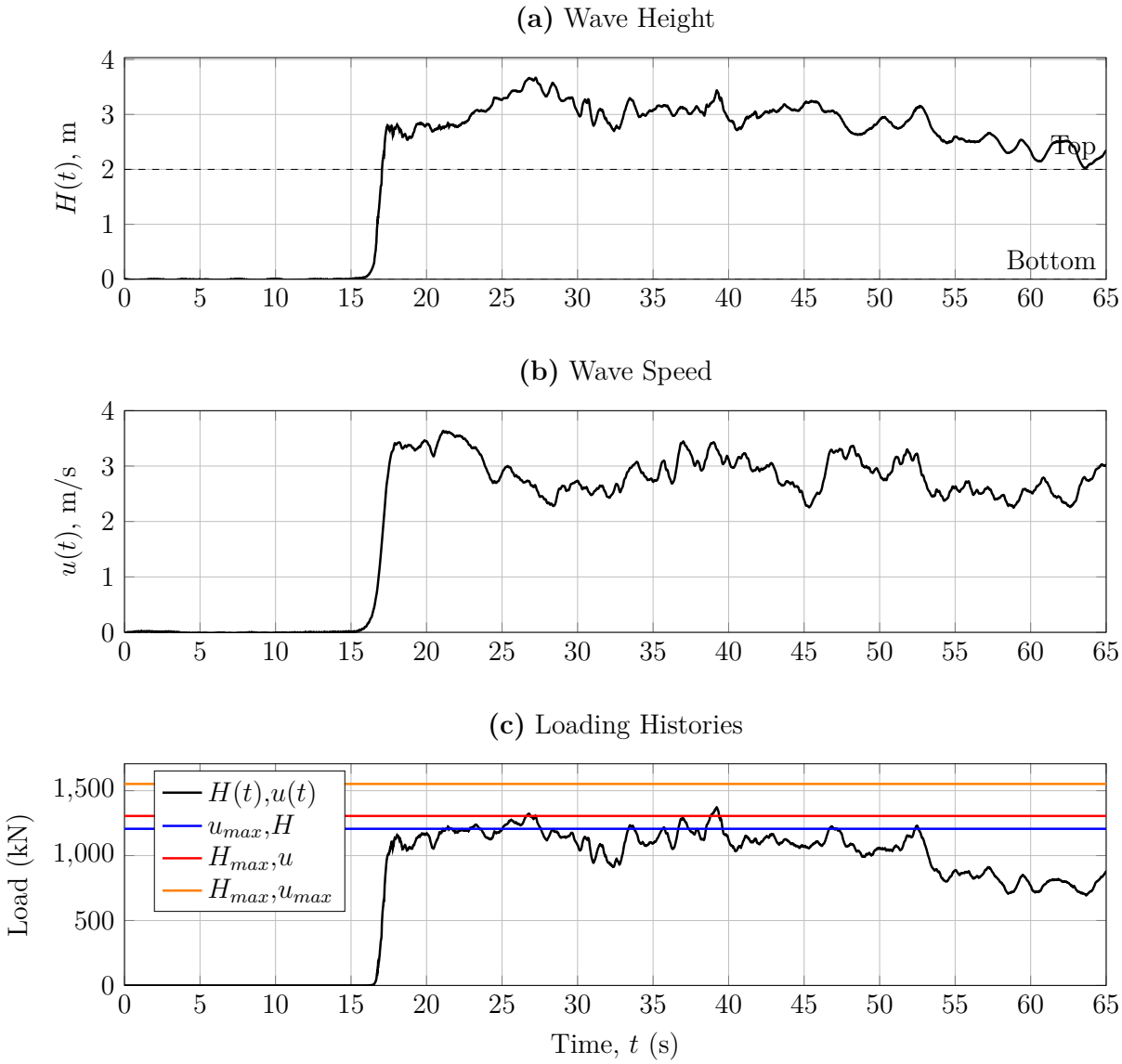

Figure 5.14: Deck-girder bridge with no clearance and 3 m wave height: (a) time history of wave height; (b) time history of wave speed; (c) time history of loading and loadings based on maxima of wave height and speed.

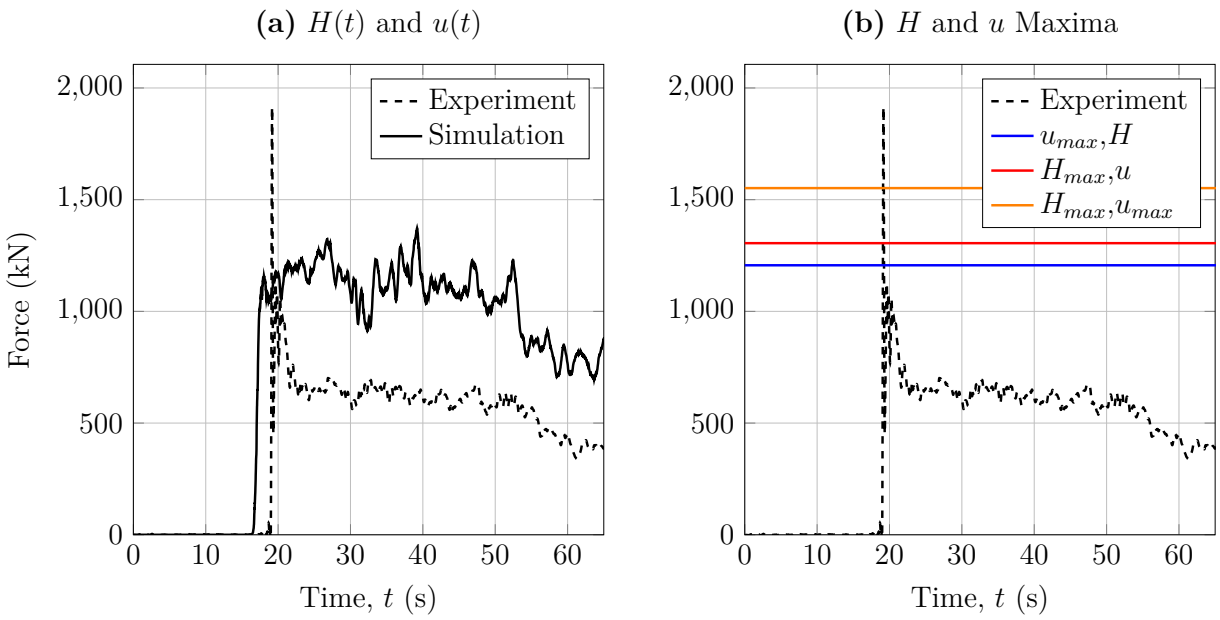

Figure 5.15: Deck-girder bridge with no clearance and 3 m wave height: (a) comparison of experimental and simulated reaction forces and (b) comparison of experimental and maxima-based reaction forces.

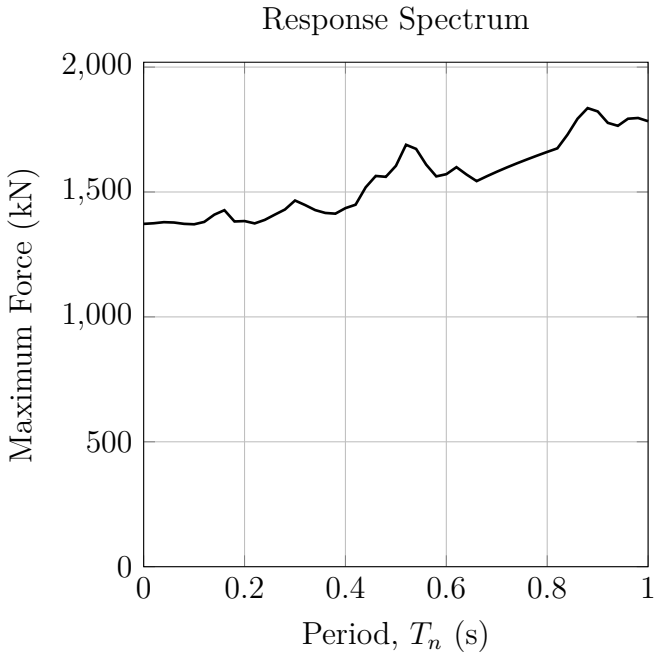

Figure 5.16: Deck-girder bridge with no clearance and 3 m wave height: response spectrum for maximum horizontal force based on time histories of wave height and speed and 5% structural damping.

6 Conclusions and Recommendations

Analyses of horizontal loads imparted on bridge superstructures were performed using a mass-spring-damper model for the bridge. With recorded time histories of tsunami wave height and speed, simple equations based on hydrostatic and hydrodynamic loads give reasonable horizontal reaction force histories when compared to experimental recordings. Conservative estimates of horizontal loads were obtained using maxima of wave height and speed in the loading equations. These estimates are important for the design and assessment of bridge response to tsunami loading without resorting to response history simulation. Simplified loading equations can also be applied for estimation of uplift and downward forces produced by tsunami loading as well as for comparison with experimental recordings.

As flexibility was introduced to the system by decreasing the spring stiffness, the maximum horizontal force developed in the spring tended to increase as the natural period of the system increased. These results indicate that bridges with flexible connections between the superstructure and substructure, or with flexible substructures, could experience higher demands than bridges that are more "rigid." Although more complex simulation models would be required in order to capture the interaction of structural flexibility with wave loading, these results are consistent with previous studies on the competing objectives of strength and stiffness for structures subjected to earthquake and tsunami hazards [15]. On the other hand, added flexibility could be beneficial for bridges, as it can make them less prone to the effects of high magnitude, high frequency impulse loadings at the onset of tsunami attack. Wave flume experiments to investigate the influence of connection flexibility on bridge response to tsunami loading have been conducted [5] and further research will be required to compare experimental results and analytical findings. The simplified modeling approach presented here will be useful for such correlations.

References

[1] M. Hayatdavoodi, B. Seiffert, and R. C. Ertekin. Experiments and computations of solitary-wave forces on a coastal-bridge deck. Part II: Deck with girders. *Coastal Engineering*, 88:210–228, 2014.

[2] J. Hoshikuma, G. Zhang, H. Nakao, and T. Sumimura. Tsunami-induced effects on girder bridges. In *Proc., Int. Symp. for Bridge Earthquake Engineering*, pages 11–23, Tokyo, Japan, 2013. Japan Association of Earthquake Engineering.

[3] H. Nakao, G. Zhang, T. Sumimura, and J. Hoshikuma. Numerical assessment of tsunami-induced effect on bridge behavior. In *Proc., Int. Symp. for Bridge Earthquake Engineering*, pages 1–13, Tokyo, Japan, 2013. Japan Association of Earthquake Engineering.

[4] D. Istrati, I. Buckle, and A. Itani. Experimental study of connection forces in bridges during tsunami inundation. PEER Annual Meeting, Berkeley, CA, 2016.

[5] D. Istrati. *Large-Scale Experiments of Tsunami Inundation of Bridges including Fluid-Structure-Interaction*. PhD thesis, University of Nevada, 2017.

[6] C. Bradner, T. Schumacher, D. Cox, and C. Higgins. Experimental Setup for a Large-Scale Bridge Superstructure Model Subjected to Waves. *Journal of Waterway, Port, and Coastal Engineering*, 137(1):3–11, 2011.

[7] J. B. Lehrman, C. Higgins, and D. Cox. Performance of Highway Bridge Girder Anchorages under Simulated Hurricane Wave Induced Loads. *Journal of Bridge Engineering*, 17(2):259–271, 2012.

[8] J. D. Bricker, K. Kawashima, and A. Nakayama. CFD analysis of bridge deck failure due to tsunami. In *Proc., International Symposium on Engineering Lessons Learned*

from the 2011 Great East Japan Earthquake, pages 1398–1409, Tokyo, Japan, 2012. Japan Association of Earthquake Engineering.

[9] M. Azadbakht and S. C. Yim. Simulation and Estimation of Tsunami Loads on Bridge Superstructures. *Journal of Waterway, Port, Coastal, and Ocean Engineering*, 141(2):04014031, 2015.

[10] M. R. Motley, H. K. Wong, X. Qin, A. O. Winter, and M. O. Eberhard. Tsunami-Induced Forces on Skewed Bridges. *Journal of Waterway, Port, Coastal, and Ocean Engineering*, 142(3):04015025, 2016.

[11] M. H. Scott, H. Yeh, and L. Cressman. UJNR Tsunami Modeling Workshop. Technical report, `https://secure.engr.oregonstate.edu/wiki/tsunamiworkshop`, 2014.

[12] M. Azadbakht and S. C Yim. Estimation of Cascadia Local Tsunami Loads on Pacific Northwest Bridge Superstructures. *Journal of Bridge Engineering*, 21(2):04015048, 2016.

[13] P. J. Lynett and M. H. Scott. Development of tsunami design guidelines for coastal bridges. Technical report, Pacific Earthquake Engineering Research Center, Berkeley, CA, 2019.

[14] M. Zhu, I. Elkhetali, and M.H. Scott. Validation of OpenSees for tsunami loading on bridge superstructures. *Journal of Bridge Engineering*, 23(4):04018015, 2018.

[15] M. H. Scott and H. B. Mason. Constant-ductility response spectra for sequential earthquake and tsunami loading. *Earthquake Engineering and Structural Dynamics*, 46(9):1549–1554, 2017.